Revised manuscript (JVI00291-19) for publication in the *Journal of Virology*

# Identification and characterization of a human coronavirus 229E nonstructural protein 8-associated RNA 3'-terminal adenylyltransferase activity

Jana Tvarogová,[a] Ramakanth Madhugiri,[a] Ganesh Bylapudi,[a] Lyndsey J. Ferguson,[b] Nadja Karl,[a,b] John Ziebuhr[a,b#]

[a]Institute of Medical Virology, Justus Liebig University Giessen, Giessen, Germany

[b]Centre for Infection and Immunity, School of Medicine, Dentistry and Biomedical Sciences, Queen's University Belfast, Belfast, United Kingdom

Running Head: RNA adenylyltransferase activity of coronavirus nsp8

**Keywords**

RNA virus, coronavirus, replication, nsp8, ribonucleotidylyl transferase, RNA 3'-terminal adenylyltransferase, poly(A) tail

# Address correspondence to John Ziebuhr, john.ziebuhr@viro.med.uni-giessen.de.

J.T. and R.M. contributed equally to this work.

Mailing address: Institute of Medical Virology, Biomedical Research Center Seltersberg, Justus Liebig University, Schubertstrasse 81, 35392 Giessen, Germany.
Phone: +49-641-9941200
Fax: +49-641-9941209
E-mail: john.ziebuhr@viro.med.uni-giessen.de

## Abstract

Coronavirus nonstructural protein (nsp) 8 has been suggested to have diverse activities, including 'noncanonical' template-dependent polymerase activities. Here, we characterized a recombinant form of the human coronavirus 229E (HCoV-229E) nsp8 and found that the protein has metal ion-dependent RNA 3'-terminal adenylyltransferase (TATase) activity, while other nucleotides were not (or very inefficiently) transferred to the 3' ends of single-stranded and (fully) double-stranded acceptor RNAs, respectively. Using partially double-stranded RNAs, very efficient TATase activity was observed if the opposite (template) strand contained a short 5' oligo(U) sequence while very little (if any) activity was detected for substrates with other homopolymeric or heteropolymeric sequences in the 5' overhang. The oligo(U)-assisted/templated TATase activity on partial-duplex RNAs was confirmed for two other coronavirus nsp8 proteins, suggesting that the activity is conserved among coronaviruses. Substitution of a conserved Lys residue with Ala abolished the *in vitro* RNA-binding and TATase activities of nsp8 and caused a non-viable phenotype when the corresponding mutation was introduced into the HCoV-229E genome, confirming that these activities are mediated by nsp8 and critical for viral replication. In additional experiments, we obtained evidence that nsp8 has a pronounced specificity for adenylate and is unable to incorporate guanylate into RNA products, which strongly argues against the previously proposed template-dependent RNA polymerase activity of this protein. Given the presence of an oligo(U) stretch at the 5' end of coronavirus minus-strand RNAs, it is tempting to speculate (but remains to be confirmed) that the nsp8-mediated TATase activity is involved in the 3'-polyadenylation of viral plus-strand RNAs.


## Importance

Previously, coronavirus nsp8 proteins were suggested to have template-dependent RNA polymerase activities resembling those of RNA primases or even canonical RNA-dependent RNA polymerases, while more recent studies suggest an essential cofactor function of nsp8 (plus nsp7) for nsp12-mediated RNA-dependent RNA polymerase activity. In an effort to

reconcile conflicting data from earlier studies, the study revisits coronavirus nsp8-associated activities using additional controls and proteins. The data obtained for three coronavirus nsp8 proteins provide evidence that the proteins share metal ion-dependent RNA 3' polyadenylation activities that are greatly stimulated by a short oligo(U) stretch in the template strand. In contrast, nsp8 was found to be unable to select and incorporate appropriate (matching) nucleotides to produce complementary RNA products from heteropolymeric and other homooligomeric templates. While confirming the critical role of nsp8 in coronavirus replication, the study amends the list of activities mediated by coronavirus nsp8 proteins in the absence of other proteins.





Journal of Virology JVI Journal of Virology

67 **Introduction**

68 Coronaviruses include important human and animal pathogens (1, 2). They have very large
69 plus-strand (+) RNA genomes of approximately 30 kilobases (kb) and, compared to most
70 other +RNA viruses, employ strategies of unusual complexity to express and replicate their
71 genomes (3-5). Over the past two decades, significant progress has been in the
72 characterization of key mechanisms and factors involved in the replication and transcription
73 of the coronavirus genome RNA (for a recent review, see (6)). Although it is now widely
74 accepted that viral RNA synthesis (and modification) is mediated by a large multi-subunit
75 protein complex (called replication-transcription complex (RTC)), our understanding of the
76 proteins involved in individual steps of viral RNA synthesis remains limited. For example,
77 there is little or no information on (i) viral (or cellular?) factors involved in 5' capping and 3'
78 polyadenylation of viral plus-strand RNAs (6, 7) and (ii) proteins that control the
79 discontinuous RNA synthesis required to produce subgenome-length negative-strand RNAs
80 carrying a 3' antileader sequence, which are subsequently used to produce mRNAs with a
81 common 5'-leader sequence that is identical to the 5' end of the genome (8, 9). It has been
82 proposed that nonstructural protein (nsp) 12, a ~105-kDa protein comprised of N-terminal
83 nucleotidyl transferase (NiRAN) (10) and C-terminal RNA-dependent RNA polymerase
84 (RdRp) (11) domains, forms a complex with nsp7 and nsp8 (12, 13) and this complex is
85 required and sufficient for template-dependent RNA synthesis *in vitro* (14). There is also
86 evidence that the fidelity of this polymerase complex is enhanced by a 5'-to-3'
87 exoribonuclease (ExoN) activity associated with the N-terminal domain of nsp14 (15, 16).
88 The proposed role of ExoN in ensuring superior RNA replication fidelity has been supported
89 by reverse genetic studies using a range of coronavirus ExoN knock-out mutants for which
90 mutator or nonviable phenotypes have been reported (16-22).
91
92 The functional characterization of individual replicase gene-encoded proteins revealed that
93 the severe acute respiratory syndrome coronavirus (SARS-CoV) nsp8 has a second
94 'noncanonical' RNA polymerase activity *in vitro* that catalyzes the production of short (≤6-nt)

oligonucleotides in a $Mn^{2+}$ ion- and template-dependent manner, reminiscent of cellular RNA primase activities (23). The short oligonucleotides synthesized by nsp8 were proposed to serve as primers for the canonical RNA polymerase (nsp12). The study also provided data to suggest that nsp8 synthesizes these oligonucleotides *de novo* and lacks the ability to extend primer/template substrates. In contrast, a subsequent study using a C-terminally $His_6$-tagged form of SARS-CoV nsp8 suggested that nsp8 (alone or in complex with nsp7) is able to extend primed RNA templates in the presence of $Mg^{2+}$, thus questioning the 'primase hypothesis' proposed earlier (23, 24). The study also postulated that the nsp(7+8) complex is capable of synthesizing substantially longer RNA products, in both *de novo* RNA polymerase and primer extension reactions (24). Similarly, *de novo* RNA polymerase activities resulting in longer 'transcripts' were suggested to be produced by different N-terminally tagged forms of the feline infectious peritonitis virus (FIPV) nsp8, based on the identification of slowly migrating [$^{32}$P]-labeled products generated in reactions supplemented with nsp8 and metal ions (12). To our knowledge, the latter two studies did not use 3'-blocked template RNAs to exclude that the radiolabeled template-length RNA products ('transcripts') observed in *de novo* polymerase assays represented 3'-extended forms of the template(s) used in these assays.

This brief overview of nsp8 *in vitro* studies performed by different laboratories with different protein constructs shows that our understanding nsp8-associated polymerase (and, possibly, other) activities is incomplete. Based on its conservation among corona- and toroviruses as well as reverse genetics and biochemical data obtained for SARS-CoV nsp8, this small protein is thought to have an important function in coronavirus and, most probably, torovirus replication. However, some of the main conclusions obtained in earlier studies remained controversial and deserve further investigation. We therefore decided to produce three coronavirus nsp8 proteins with their authentic amino termini using previously established protocols. C-terminally $His_6$-tagged wildtype and mutant forms of HCoV-229E nsp8 (the latter containing Lys-to-Ala substitutions corresponding to previously characterized replacements

in SARS-CoV nsp8) as well as C-terminally $His_6$-tagged wildtype forms of SARS-CoV and FIPV nsp8 were purified to apparent homogeneity. The characterization of (putative) HCoV-229E nsp8 polymerase activities, RNA substrate and nucleotide preferences, RNA-binding activities, and metal ion requirements leads us to conclude that the wildtype protein (but not the nsp8_K3711A mutant) has RNA 3'-terminal adenylyltransferase (TATase) activity if incubated with single-stranded and completely double-stranded substrates. This activity can be significantly stimulated by providing a short oligo(U) stretch as a template. Unlike previous studies, we failed to obtain evidence for a canonical (i.e., high-fidelity and template-dependent) RNA-dependent RNA polymerase activity for this HCoV-229E homolog, which is in line with the protein's pronounced specificity for adenylate. Using a substrate described in a previous study, HCoV-229E nsp8 was found to generate products that corresponded to those obtained previously with SARS-CoV-nsp8 (24). However, based on additional data obtained for 3'-blocked versions of the test substrate, we arrived at different conclusions regarding the identities of some of the products. Taken together, our data lead us to suggest that nsp8 acts as an oligo(U)-templated polyadenylyltransferase but also has robust (mono/oligo)adenylate transferase activities when incubated with single-stranded and blunt-ended double-stranded RNAs. We think that this activity explains most of the data published previously on coronavirus nsp8 homologs, even though additional experiments and controls would be desirable to further substantiate this hypothesis.

## Results

**Expression and purification of recombinant HCoV-229E nsp8**. To produce a recombinant form of HCoV-229E nsp8 with its authentic N-terminus, an expression strategy introduced by Gohara *et al*. was used (25) (see Materials and Methods). Briefly, the HCoV-229E nsp8 coding sequence (fused to an N-terminal Ub tag and a C-terminal hexahistidine tag, Ub-nsp8-$CHis_6$) was inserted into a pASK3-derived plasmid (26) downstream of a tetracycline-inducible promoter. Coexpression of Ub-nsp8-$CHis_6$ and Ubp1 resulted in proteolytic cleavage at the ...LRGG↓SVAS... site between the Ub-moiety and the nsp8 sequence in the Ub-nsp8-$CHis_6$ fusion protein, resulting in the release of a C-terminally $His_6$-tagged form of nsp8 with its correct N-terminus ($NH_2$-SVAS...) (Fig. 1A). The protein was purified by Ni-NTA affinity and anion exchange chromatography as described in Materials and Methods. As shown in Fig. 1B, induction of expression in *E. coli*-TB1 pCG1 cells with AHT gave rise to an extra protein of approximately 22 kDa which corresponded well with the molecular mass of 22 kDa calculated for the nsp8-$CHis_6$ protein (Fig. 1B, lanes 1 and 2). Using a two-step protocol, HCoV-229E nsp8 and the (mutant) nsp8_K3687A and nsp8_K3711 proteins, respectively, could be purified in sufficient amounts for biochemical studies and proved to be stable upon storage at -20°C (Fig. 1A, Fig. 1B, lanes 3 to 5).

**Terminal adenylyltransferase (TATase) activity of HCoV-229E nsp8.** Preliminary experiments using HCoV-229E nsp8 (Fig. 2 and data not shown) revealed the production of radiolabeled products when the protein was incubated with synthetic oligoribonucleotide substrates in the presence of $\alpha$-[$^{32}$P]-ATP, confirming that the purified protein was active. To optimize reaction conditions for subsequent studies, we used $U_{18}$ as a test substrate and incubated the reaction mixtures at 30°C for 60 minutes under varying conditions with respect to (i) nsp8 concentration, (ii) NaCl concentration, (iii) identities and concentrations of metal ions, (iv) pH, and (v) ribonucleotide concentrations. Based on these experiments (Fig. 2 and data not shown), we decided to use the following optimized ('standard') reaction buffer in subsequent experiments: 50 mM Tris-Cl, pH 8.0, 50 mM NaCl, 1 $MgCl_2$, 1% Triton X-100, 1

172 mM DTT, 4.5 % glycerol, 1 μM substrate RNA, 100 μM of the indicated NTP(s), 0.17 μM of
173 the indicated [α-$^{32}$P] NTP(s) (3000 Ci/mmol), and 2 μM nsp8. Consistent with previous
174 studies of the SARS-CoV nsp8 (23, 24), the data revealed that HCoV-229E nsp8 activity
175 required the presence (of moderate concentrations) of $Mg^{2+}$ or $Mn^{2+}$ ions (Fig. 2B). High
176 concentrations of these ions inhibited activity, while other metal ions failed to support nsp8
177 activity (Fig. 2C). HCoV-229E nsp8 activity proved to be sensitive to salt concentrations
178 above 50 mM (Fig. 2A).
179
180 In the presence of α-[$^{32}$P]-ATP (only), radiolabeled products with sizes that exceeded those
181 of the substrate RNAs were found to be generated. These larger-than-expected products
182 were obtained with both the homopolymeric $U_{18}$ and the heteropolymeric substrate RNA
183 KR07 (5'-UAAUGGAACGGUUUCGAUAUGGAUACAC-3', representing the 3' end of the
184 HCoV-229E genome RNA) (Fig. 2C), suggesting that (i) the protein has adenylyltransferase
185 activity and (ii) the products likely represent 3'-polyadenylated forms (rather than
186 complementary copies) of the substrate RNAs used.
187
188 To corroborate the idea of HCoV-229E nsp8 acting as an RNA 3'-terminal ribonucleotidyl
189 transferase (TNTase), we decided to include 3'-biotinylated RNA substrates that lacked a
190 free 3'-hydroxyl group as controls and performed reactions containing just a single
191 nucleotide, i.e., (i) ATP and [α-$^{32}$P] ATP, (ii) CTP and [α-$^{32}$P]-CTP, (iii) UTP and [α-$^{32}$P]-UTP,
192 and (iv) GTP and [α-$^{32}$P]-GTP, respectively. As shown in Fig. 3, radiolabeled AMP was
193 efficiently incorporated into products by HCoV-229E nsp8 if the reactions were performed
194 with substrate RNAs carrying unmodified 3' ends, while no radiolabeled products were
195 generated from 3'-biotinylated substrate RNAs in the presence of 100 μM ATP and 0.17 μM
196 [α-$^{32}$P] ATP (Fig. 3A and B, lanes 2 and 8). With some (but not all) substrate RNAs, a rather
197 inefficient incorporation of CMP was observed (Fig. 3A, lanes 4 and 10; Fig. 3B, lane 4),
198 while there was (nearly) no incorporation of GMP and UMP into any of the test substrates
199 used (Fig. 3). Taken together, these data provide strong support for the proposed RNA 3'-

ribonucleotidyl transferase activity of HCoV-229E nsp8 and reveal a pronounced preference for ATP in the transfer reaction, irrespective of the type of substrate RNA used (homopolymeric or heteropolymeric). In an additional set of experiments using dATP instead of ATP, we found that [$\alpha$-$^{32}$P]-dAMP was not incorporated into any of the substrate RNAs used (data not shown), confirming that the nsp8-mediated RNA 3' polyadenylation reaction requires the presence of a ribose-2' hydroxyl group.

Next, we explored possible preferences of the nsp8 TATase activity for specific substrates and asked the question of whether the presence of specific 3'-terminal nucleotides affects the nsp8 TATase activity. The nucleotide sequence of one of the substrates corresponded to that of the 3' end of the HCoV-229E genome (KR07). In addition, we used a range of KR07 derivatives carrying replacements of the 3' cytidylate with adenylate, uridylate, and guanylate, respectively (Fig. 4A). Reactions were performed under the optimized conditions described above and in the presence of 100 μM ATP and 0.17 μM [α-$^{32}$P] ATP. Compared to the TATase activity obtained with KR07, nucleotide replacements of the 3'-terminal cytidylate resulted in increased TATase activities, with KR07_C28A and KR07_C28G representing the best substrates. Similarly, using another substrate, JZR3, replacements of the 3'-cytidylate with adenylate or guanylate resulted in superior activities (Fig. 4C, lanes 2 and 5). These data suggest that, at least *in vitro*, substrates with a 3'-terminal purine (with A being preferred over G) are polyadenylated more efficiently than substrates carrying a 3'-terminal pyrimidine.

**Activity of HCoV-229E nsp8 on partial-duplex RNA substrates**. The data presented above suggest that HCoV-229E nsp8 is able to 3'-polyadenylate ssRNA substrates with diverse sequences/structures if these substrates contain a free 3'-hydroxyl group. Apparently, the protein did not require a primer/template hybrid (or a template) to generate radiolabeled RNA products, unlike what was suggested in earlier studies in which SARS-CoV nsp8 appeared to produce radiolabeled RNA products in a template-dependent manner indicative of both *de novo* and primer-dependent RNA polymerase activities (23, 24). In an

effort to reconcile the previously published SARS-CoV nsp8 data with data obtained for HCoV-229E nsp8, a series of *in vitro* activity assays was performed using substrate and reaction conditions corresponding to those described by te Velthuis *et al.* (24). Of note, the nucleotide sequences of the partially double-stranded RNA substrate (named KR01/JTR1 in the present study) were identical to those of the SAV556/SAV557 substrate used in the previous study. In the presence of 50 μM ATP and 0.17 μM [$\alpha$-$^{32}$P] ATP, HCoV-229E nsp8 was revealed to produce multiple radioactively labeled products of ≥40 nts, suggesting efficient 3' polyadenylation of one or both strands of KR01/JTR1 (Fig. 5B, lane 4). Similar products were obtained in the presence of 50 μM ATP, 50 μM GTP, and 0.17 μM [$\alpha$-$^{32}$P] ATP (Fig. 5B, lane 2). In striking contrast, no radiolabeled products were detected if the reaction was performed in the presence of 50 μM ATP, 50 μM GTP and 0.17 μM [$\alpha$-$^{32}$P] GTP (Fig. 5B, lane 3). These data show that nsp8 is unable to incorporate GMP into reaction products, which strongly argues against a 'true' copy process of the C/U sequence present in the 'primed' RNA substrate KR01/JTR1 to generate a G/A sequence. This conclusion is further supported by data obtained in a reaction containing 50 μM ATP and 0.17 μM [α-$^{32}$P] ATP in which prominent products of ≥40 nts that comigrated with the products seen in lane 2 were observed while no labeled product was detected in a reaction containing 50 μM GTP and 0.17 μM [α-$^{32}$P] GTP, even though the template contained a C at the first position (Fig. 5B, compare lanes 4 and 5). Interestingly, the protein failed to produce radiolabeled products when KR01/JTR1-b hybrid RNA was used as a substrate (Fig. 5B, lanes 6 to 9). The fact that 3' biotinylation of the bottom strand JTR1-b nearly completely abolished TATase activity led us to conclude that the labeled products seen in lanes 2 and 4 represent 3'-polyadenylated forms of the bottom (JTR1) rather than the top strand (KR01). Also, the data obtained in this and subsequent experiments (Fig. 6 and data not shown) suggest that, unlike suggested previously by others (24), radiolabeled products of the nsp8 activity do not represent 3'-extended primers resulting from an ATP- and GTP-dependent copy process of the $(CU)_{10}$-containing template sequence. Instead, they represent 3' mono-, oligo- and polyadenylated variants of the bottom strand of the partially double-stranded RNA hybrid used in the

256 respective experiment. The data also suggest that, with one important exception (see below),
257 nsp8 TATase activity prefers 'blunt' over 'recessive' 3' ends in partially double-stranded
258 substrate RNAs.
259
260 **HCoV-229E nsp8 has oligo(U)-assisted TATase activity**. Although we failed to obtain
261 evidence for 'generic' RNA template-dependent RNA polymerase activities, a number of
262 preliminary experiments (Fig. 5 and data not shown) indicated that the 3'-adenylation activity
263 of nsp8 on double-stranded RNA may be affected by the presence or absence of specific 5'
264 single-stranded regions in the bottom strand. To explore more directly the role of single-
265 stranded RNA regions with varying sequences located opposite the strand with ongoing 3'
266 adenylation, partially double-stranded RNAs were designed in which the 'top' strand (KR07)
267 was hybridized to a complementary RNA called KR07comp-b. In this case, the 'bottom'
268 strand was 3'-biotinylated to block any potential nsp8-mediated 3'-adenylation of this strand.
269 In addition to this basic construct, a range of 3'-biotinylated bottom strands with different 5'
270 overhangs including $U_{10}$, $C_5U_5$, $U_5C_5$, $C_{10}$, and $A_{10}$, respectively, were synthesized and
271 hybridized to KR07 (Fig. 6A). As controls, a number of dsRNAs in which both the top and the
272 bottom strand were 3'-biotinylated were included in these experiments (Fig. 6A).
273
274 In line with previous experiments, HCoV-229E nsp8 was found to have robust TATase
275 activity using the single-stranded RNA KR07 as a substrate (Fig. 6B, lane 3). A similar
276 TATase activity was observed for the KR07/KR07comp-b RNA hybrid, suggesting that (fully)
277 double-stranded RNA can be equally efficiently 3'-polyadenylated by nsp8 (Figure 6B, lane
278 4). As shown before, 3'-biotinylated forms of single- or double-straded RNA substrates were
279 not polyadenylated (Fig. 6B, lanes 2, 5, and 6). Maximum 3'-polyadenylation of the top strand
280 was observed for an RNA hybrid in which the bottom strand had an unpaired 5' $U_{10}$ overhang
281 (Figure 6B, lane 8), and only slightly lower activities were observed for 5' overhangs with
282 $U_5C_5$ and $C_5U_5$ sequences, respectively (Fig. 6B, lanes 7 and 9). In contrast, we failed to
283 detect TATase activity for dsRNA substrates containing 5' $A_{10}$ and $C_{10}$ overhang regions,

284 respectively (KR07/$A_{10}$KR07comp-b, KR07/$C_{10}$KR07comp-b) (Fig. 6B, lanes 10 and 11). For
285 the latter two substrates, labeled products could also not be detected if the 'matching'
286 nucleotides, UTP and GTP, respectively, were included in the reaction (Fig. 6C). Taken
287 together, the data show that HCoV-229E nsp8 TATase activity is strongly stimulated by the
288 presence of a short (≥5-nt) oligo(U) stretch in the opposite strand, suggesting that nsp8 uses
289 the oligo(U) stretch (or a part of it) as a template. To corroborate this hypothesis, we modified
290 the KR01-containing substrates used in the previous experiment (Fig. 6) to include longer 5'
291 single-stranded regions in the bottom strand, (i) a mixed $(UC)_{10}$ sequence and (ii) a
292 homooligomeric $U_{20}$ sequence (Figure 7A). If the KR01 3' end was blocked with biotin, no
293 radiolabeled product was generated, while TATase activity was readily detectable for KR01
294 with a free 3'-hydroxyl group (Fig. 7B, compare lanes 2 and 3). There was no detectable
295 activity using a substrate containing a mixed $(CU)_{10}$ sequence in the 5' single-stranded region
296 of the bottom strand (Fig. 7B, lane 4), while very efficient TATase activity was observed for
297 an RNA hybrid containing an unpaired 5' $U_{20}$ sequence in the bottom strand (Fig. 7B,
298 compare lanes 4 and 7), providing additional evidence for the proposed poly(U)-templated
299 TATase activity of nsp8. In line with previous experiments (see above), we failed to detect
300 radiolabeled products in reactions using 3'-biotinylated dsRNA substrates (KR01-b/JTR1-b,
301 KR01-b/$U_{20}$JTR1comp-b), confirming the requirement of a free 3' hydroxyl group for nsp8
302 TATase activity (Fig. 7B, lanes 4 and 5; Fig. 6).
303
304 Next, we tested if SARS-CoV nsp8 and FIPV nsp8 display the same poly(U) template-
305 assisted TATase activity described above for the HCoV-229E homolog. To this end,
306 recombinant forms of SARS-CoV and FIPV nsp8 were produced in *E. coli* (see Materials and
307 Methods) and used in reactions supplemented with 2 μM of the appropriate nsp8, 50 mM
308 NaCl, 1 mM $MgCl_2$, 100 μM ATP and 0.17 μM [$\alpha$-$^{32}$P] ATP and 1 μM substrate RNA (Fig.
309 8A). Using a partially double-stranded RNA substrate with an unpaired 5' $U_{20}$ sequence in the
310 bottom strand, we found that all three nsp8s displayed robust TATase activity resulting in a
311 product of ≥40 nt (Figure 8B, lane 3, 5, and 7). Among the three coronavirus nsp8s used in

this experiment, SARS-CoV nsp8 displayed the most efficient TATase activity with this particular substrate (Fig. 8B, lane 7). Together, these data suggest that oligo(U) template-assisted TATase activity is a conserved feature of coronavirus nsp8 proteins.

**Role of conserved Lys residues in HCoV-229E nsp8-mediated RNA-binding and TATase activities, and viral replication**. Previous structural and biochemical studies identified a number of residues to be essential for nsp8 'polymerase/primase' activity, protein-protein and protein-RNA interactions, respectively (12-14, 23, 24). To assess the potential role in TATase activity of two HCoV-229E nsp8 residues equivalent to conserved Lys residues shown previously to be important for SARS-CoV nsp8 primase activity and SARS-CoV replication (14, 23), we produced mutant forms of HCoV-229E nsp8 in which pp1a residues Lys-3687 and Lys-3711, respectively, were replaced with Ala (Fig. 1). The proteins were produced in *E. coli* and purified to apparent homogeneity using metal-ion affinity and anion-exchange chromatography (Fig. 1B). TATase activities of the mutant proteins were determined using the reaction conditions established for the wildtype enzyme; and KR07 and $U_{18}$ were used as test substrates in these assays. As shown in Fig. 9, no TATase activity was detected for the nsp8_K3711A protein while nsp8_K3687A retained its TATase activity on the two RNA substrates used in this experiment (Fig. 9A and B). Next, we determined the RNA-binding activities of the wildtype and mutant nsp8 proteins using a range of RNAs ($A_{18}$, $U_{18}$, $C_{18}$ and KR07) (see Materials and Methods). As shown in Fig. 9 (C and D), nsp8_K3687A bound RNA less efficiently than the wildtype protein. The reduced RNA-binding activity of nsp8_K3687A was particularly evident using $A_{18}$ and $C_{18}$ (Fig. 9C), while the protein retained RNA-binding activity to $U_{18}$ and KR07 (Fig. 9C and D). In contrast, the K3711A substitution abolished the RNA-binding activity of the protein completely (Fig. 9C and D), suggesting that the lack of TATase activity was probably caused by insufficient RNA-binding capacity of this protein.

In a final set of experiments, we examined possible effects of the pp1a/pp1ab K3687A and K3711A substitutions in the context of viral replication in cell culture. Full-length HCoV-229E genome RNAs containing the desired mutations were generated using the reverse genetics system developed by Thiel *et al.* (27). Following cotransfection of Huh-7 cells with 1.25 µg of *in vitro*-transcribed 5'-capped full-length HCoV-229E RNA (wildtype and nsp8 mutants, respectively) along with 0.75 µg N mRNA, the cells were incubated at 33°C. Determination of virus titers in the cell culture supernatants collected at 72 h p.t. revealed that wt HCoV-229E was readily recovered with titers of $>10^6$ pfu/ml while no viable viruses could be rescued after transfection of mutant RNAs (HCoV-229E_K3687A and _K3711A, respectively), suggesting critical roles of nsp8-mediated activities in viral replication.

## Discussion

Although previous studies on coronavirus nsp8 proteins (including their complexes with nsp7) were focused on recombinant forms of nsp8 of only two viruses, SARS-CoV and FIPV, partly inconsistent or controversial information was obtained in several instances (6, 12, 14, 23, 24). With regard to enzymatic activities and possible roles in viral RNA synthesis, at least four functions have been suggested for nsp8. The protein was shown to be an essential cofactor (together with nsp7) for RdRp activity *in vitro*. Additional functions were suggested to include (i) processivity factor for the viral RdRp (in a hexadecameric complex with nsp7), (ii) 'noncanonical' RdRp (primase) activity, and (iii) primer-dependent and *de novo* RdRp activities (alone or in complex with nsp7) (12-14, 23, 24). Possibly, some of the discrepant findings of these studies may be explained by the presence of a few extra residues in the respective protein constructs (6). And indeed, there is evidence that the presence and identities of N-terminal tags may affect the activities of SARS-CoV and FIPV nsp8 (12, 24). In an effort to revisit the diverse polymerase activities reported previously for two coronavirus nsp8 proteins, we decided to focus on the isolated nsp8 protein by characterizing the activities of the HCoV-229E nsp8 (representing the genus *Alphacoronavirus*) and, subsequently, extended major findings arising from this work to previously characterized nsp8 homologs from SARS-CoV (genus *Betacoronavirus*) and FIPV (genus *Alphacoronavirus*). To produce and purify these proteins in an active form, we took advantage of a previously established system suitable to generate C-terminally $His_6$-tagged forms of nsp8 with their authentic N-terminal residues in a T7 polymerase-free system, thereby eliminating the risk of T7 RNA polymerase contamination which may interfere with subsequent analyses of viral RdRp activities produced in *E. coli* (24, 25). The proteins were purified from *E. coli* by metal-ion affinity and anion-exchange chromatography and characterized *in vitro* using protocols optimized in this study.

Using SARS-CoV and HCoV-229E nsp8, respectively, we failed to obtain evidence for primase activity for these proteins (that is, template-dependent *de novo* polymerase activity

resulting in short oligonucleotides) on any of the substrates used, which is in agreement with a study by Subissi *et al.* (14) but contradicts an earlier report (23). We however found that HCoV-229E nsp8 transfers (ribo)nucleotides to the 3' end of substrate RNAs, with ATP being the clearly preferred nucleotide. Importantly, this activity was not detectable if substrates were used in which the 3'-hydroxyl group was blocked, thus essentially excluding template-dependent *de novo* polymerase activities being involved in the production of the radiolabeled products obtained in our assays. Also, the vast majority of products was larger than the substrates used, and virtually identical products were generated from a partially double-stranded RNA containing a single-stranded heteropolymeric (C/U) sequence in reactions containing either ATP alone or ATP in combination with GTP, arguing against a template-dependent copy process being involved in the production of the labeled RNAs seen in the autoradiograms (Fig. 5). The latter hypothesis is supported by the lack of radiolabeled RNAs being produced if the 3' end of the bottom strand was blocked with biotin (KR01/JTR1-b), indicating that essentially all radiolabeled products seen for KR01/JTR1 in Fig. 5 (lanes 2 and 4) were produced by 3' polyadenylation of the bottom strand JTR1 (i.e., at the substrate's blunt end) rather than a copy process of the template, resulting in the 3' extension of the top strand KR01 (to fill up the 3' recessive end of the substrate).

A very weak 3' extension of single-stranded substrate RNAs was also observed in the presence of CTP and UTP, respectively, while there was no detectable incorporation of GTP in any of the substrates used (Figs. 3 and 5). The nucleotide selectivity of the nsp8-mediated terminal transferase activity resembles that of eukaryotic poly(A) polymerases (PAPs), which are known to be highly specific for ATP (28, 29). The efficient 3'-terminal polynucleotidylation of RNA substrates by PAPs in the presence of ATP (but not CTP, UTP, and GTP, respectively) has been suggested to involve nucleotide base stacking (see below). PAPs have been reported to exhibit 800-fold higher catalytic efficiencies with ATP compared to GTP (30). Both the different electrostatic properties and shapes of the two purine nucleotides were suggested to be involved in the distinct binding and use of ATP by PAPs (31, 32).

406 Based on the data obtained in this study, it seems reasonable to suggest that coronavirus
407 nsp8 homologs are RNA-specific TATases that probably act in a distributive manner.
408
409 Similar to cellular PAPs, many viral RNA polymerases, including picornavirus, calicivirus,
410 flavivirus, nodavirus, alphavirus, and bacteriophage $\phi$6 polymerases, have been reported to
411 add nontemplated nucleotides to the 3' ends of RNA products and it has been suggested that
412 the addition of a few extra nucleotides reflects an intrinsic terminal transferase activity of
413 (some of) these RdRps (33-41). These studies also showed that the TNTase activity requires
414 the presence of a 3'-hydroxyl group, as confirmed by experiments using blocked 3' ends,
415 which abolished this activity (40-42). Similarly and although not apparently related to viral
416 RdRp, the HCoV-229E nsp8 was shown to have TATase activity on homopolymeric and
417 heteropolymeric RNA substrates unless their 3' ends were blocked by 3' biotinylation (Fig. 3,
418 6, 7, 8). The nsp8-associated RNA 3' nucleotidyl terminal transferase activity displayed a
419 strong preference for ATP (over CTP and UTP), while GTP and dATP were not incorporated.
420
421 In previous studies, metal ions were demonstrated to affect nucleotide selectivity of poliovirus
422 $3D^{pol}$ *in vitro* (33). The use of $Mn^{2+}$ was found to relax nucleotide selectivity, resulting in
423 decreased RdRp fidelity (33, 43, 44). Nucleotide misincorporations and pronounced primer
424 cleavage occurred in the presence of $Mn^{2+}$ but not (or much less so) in the presence of $Mg^{2+}$
425 ions (33). $Mn^{2+}$ ions were also reported to affect alphavirus nsP4 (RdRp) TATase activity
426 (39). Because of these special effects of $Mn^{2+}$ ions when used at (nonphysiologically) high
427 concentrations, we decided to use $Mg^{2+}$ ions in (almost all) the HCoV-229E nsp8 activity
428 assays included in this study, even though $Mn^{2+}$ was confirmed to be equally effective in
429 supporting HCoV-229E nsp8-mediated TATase activity (Fig. 2B). Our decision to use of $Mg^{2+}$
430 instead of $Mn^{2+}$ ions was also prompted by data obtained in a previous study in which a
431 sequence-specific (yet low-fidelity) RdRp activity mediated by SARS-CoV nsp8 was
432 observed in reactions containing $Mn^{2+}$ ions (23), while this particular nsp8-associated activity

433 was no longer observed in a more recent study using $Mg^{2+}$ ions as metal ion cofactor in
434 RdRp assays including nsp8 (14).
435
436 Although this remains to be formally proven, it is tempting to suggest that the TATase activity
437 established in this study for HCoV-229E nsp8 may have a role in the 3'-polyadenylation of
438 viral RNAs. It has been confirmed for bovine coronavirus (BCoV) that viral plus-strand RNAs
439 are 3'-polyadenylated, while the 5' ends of negative strands contain a poly(U) track of 9-26
440 nts (45). The efficient nsp8-mediated 3'-polyadenylation of substrate RNAs in the presence of
441 a 5'-oligouridylated template supports the idea that nsp8 may have functions that resemble
442 those of cellular PAPs (see below). Even though crystal structures of SARS-CoV and FIPV
443 nsp8 have been reported (12, 13), the structural basis for the selective use of ATP for the
444 nsp8-associated terminal transferase activity remains to be established, for example, by
445 further structural studies of nsp8 in the presence of ATP analogs. Based on previous studies
446 on cellular PAPs (which, however, are not evidently related to coronavirus nsp8 proteins), it
447 seems safe to predict that multiple interactions are required for NTP selectivity, RNA
448 substrate binding and catalysis (30).
449
450 With respect to substrate specificity, we were interested to examine if (and to what extent)
451 the identities of the 3'-terminal nucleotides affect the HCoV-229E nsp8-mediated TATase
452 activity. We found that substitution of the 3'-terminal cytidylate present in KR07 and JZR3,
453 respectively, with adenylate resulted in increased nsp8 TATase activities (Fig. 4B and C).
454 Also in the presence of a 3'-terminal guanylate the nsp8 TATase activity was enhanced,
455 suggesting that purines are preferred over pyrimidines at the 3'-terminal position. Similar
456 observations were previously made for the TNTase activity of the HCV RdRp (35), where a
457 C-to-G substitution at the 3'-terminal position resulted in enhanced 3' adenylation. Early
458 studies performed in the 1960s proposed differential stacking interactions between different
459 types of nucleobases to be responsible for this preference: purine-purine > purine-pyrimidine
460 > pyrimidine-pyrimidine (46-48). Theoretical studies indicated that A-A stacking (purine-

461 purine) is more favorable than A-C stacking (purine-pyrimidine) (49, 50). As mentioned
462 above, nsp8 TATase activity was found to be increased if the 3'-terminal pyrimidine
463 (cytidylate) present in two oligonucleotide substrates was substituted with purine (A or G)
464 (Fig. 4B and C) while a moderate (or no) stimulation of activity was observed when the
465 cytidylate was replaced with another pyrimidine (uridylate). The effects observed for 3'-
466 terminal nucleotide substitutions support the idea that differential base-stacking interaction
467 may have a role in the initiation of 3' polyadenylation. Similar to the observations made in our
468 study, a 10-fold lower catalytic efficiency was reported for a cellular PAP using an $A_{18}$
469 substrate in which the 3'-terminal A was substituted with C ($A_{17}C$) (51). In line with this
470 interpretation, we found that replacements of the penultimate nucleotide had no detectable
471 effect on nsp8 TATase activity (data not shown).
472
473 In the context of an earlier study addressing possible primer-dependent and *de novo* RdRp
474 activities of the SARS-CoV nsp8 and an nsp7-nsp8 complex, evidence was presented that (if
475 a primer/template complex is provided) nsp8 is able to generate radiolabeled RNAs with
476 sizes that exceed those of the template, suggesting nontemplated 3'-TNTase activity (24).
477 This observation is consistent with what we propose here for the HCoV-229E nsp8 homolog.
478 In contrast, however, our data do not support the template-dependent copy process
479 described in that earlier study. Our data rather suggest that the near-substrate-length labeled
480 products observed in these experiments represent 3'-mono- or oligoadenylated forms of the
481 template strand. To test this hypothesis, we used the primed template described previously
482 (24) and analyzed the radiolabeled products generated by nsp8 in the presence of different
483 (combinations of) nucleotides. Labeled products could only be detected if [$^{32}$P]-ATP was
484 included in the reaction while [$^{32}$P]-GTP was not incorporated into any of the products,
485 thereby ruling out the possibility that the labeled RNA product represented a copy of the
486 $(CU)_{10}$ template (Fig. 5, 6, and data not shown). We also observed that, at low ATP
487 concentrations, only one major product (of approximately substrate length and probably
488 representing a 3'-monoadenylated RNA) was produced, while higher ATP concentrations

(50-100 μM) resulted in polyadenylated products. Importantly, no such products were observed in the presence of [$\alpha$-$^{32}$P] GTP (Fig. 5 and data not shown), once again supporting the adenylate-specific 3'-terminal ribonucleotidyl transferase activity established in this study.

To address possible roles of specific RNA structures and sequences in supporting the TNTase activity of nsp8, a series of partial-duplex RNAs with one strand representing the 3'-end of the HCoV-229E genome and the other representing the complementary 5' end of the viral antigenome (with and without 5' single-stranded tails) were used in activity assays (Fig. 6A). Using an RNA hybrid containing a 5' overhang with a short oligo(U) stretch ($U_{10}$, $U_5C_5$, and $C_5U_5$, respectively), a very efficient polyadenylation of KR07 was observed, while nearly no TATase activity was observed if the partially double-strand RNAs contained 5'-tails with $A_{10}$ or $C_{10}$ sequences in the bottom strand (Fig. 6B). The same result was obtained in reactions in which the appropriate complimentary nucleotides (UTP and GTP, respectively) were included in the respective reactions (Fig. 6C), again confirming the nucleotide selectivity of nsp8. Furthermore, the data show that HCoV-229E nsp8 TATase is equally active on single-stranded and (the blunt ends of) double-stranded RNA substrates (Fig. 6B, lanes 3 and 4), whereas recessive 3' ends in partially double-stranded RNAs are clearly disfavored (Fig. 5 and 6), unless the bottom strand contains a stretch of uridylates. While it is clear that the nsp8 TATase does not strictly require an oligo(U) template, the activity was greatly stimulated by the presence of a single-stranded oligo(U) sequence opposite the 3'-polyadenylation site, with $U_{5\text{-}10}$ stretches stimulating polyadenylation activity most efficiently. Interestingly, the position of the $U_5$ sequence in the mixed sequence ($C_5U_5$ or $U_5C_5$) was not critical, possibly indicating low processivity and repeated use of the oligo(U) template. The situation appeared to be different if the 5' oligo(U) tail was extended up to 20 nucleotides. In this case, a rather defined product was observed which was not efficiently extended beyond template length (42 nts), possibly caused by the lack of a suitable oligo(U) template once an extended (and thus stable) A-U base-paired structure had been formed by the 3'-polyadenylation reaction.

517

518 Based on the data presented in this study, it seems reasonable to suggest a model in which
519 the nsp8-mediated TATase (in conjunction with other RTC components) acts to 3'
520 polyadenylate genomic RNA and sg mRNAs in an oligo(U)-assisted manner. If confirmed,
521 this mechanism would resemble the mechanisms (including polyadenylation signals)
522 employed by negative-strand RNA viruses to produce polyadenylated mRNAs (52-55) and
523 mechanisms proposed for the poliovirus polymerase (56-58), while cellular PAPs generally
524 add poly(A) tails in a template-independent manner and depend on specific polyadenylation
525 signals (59). The factors and mechanisms that drive and regulate 3'-poly(A)-tailing of
526 coronavirus plus-strand RNAs are currently unclear and deserve further investigation.

527

528 In a previous study, the SARS-CoV nsp8 Lys-58 residue was implicated in the dsRNA-
529 binding activity of the nsp7-nsp8 complex (13). We replaced the homologous Lys residue in
530 the HCoV-229E nsp8 (K3687A) and examined the RNA-binding and TATase activities of this
531 protein. Consistent with data obtained for the corresponding SARS-CoV nsp8 mutant
532 nsp8_K58A (13, 14, 24), RNA-binding activity of HCoV-229E nsp8_K3687A was found to be
533 reduced by approximately 50% (Fig. 9C and D). Despite this reduced RNA-binding affinity,
534 the TATase activity of nsp8_K3687A was not affected or even higher than that of the
535 wildtype protein (Fig. 7A and B). Earlier studies reported a complete abolishment of nsp8
536 primase and polymerase activities for the equivalent substitution in the SARS-CoV nsp8
537 (K58A) (23, 24). Subsequently, the same replacement was shown to abolish *de novo*
538 initiation while it retained significant primer extension activity in polymerase assays of the
539 nsp7/nsp8/nsp12 complex (14). Although the basis of these differential effects are currently
540 unclear, the data obtained in these different virus systems and assays lead us to suggest
541 that this particular substitution retains (some) *in vitro* activities. The remaining ~50% RNA-
542 binding affinity of HCoV-229E nsp8_K3687A was probably sufficient to retain TATase
543 activity, while the SARS-CoV equivalent retained some of its capacity to support the
544 polymerase activity of the nsp7/8/12 complex (14). However, these functional defects

545 resulted in non-viable viruses in both cases (no RNA accumulation and virus reproduction)
546 (14), reinforcing the important role of a fully functional nsp8 in viral replication.
547
548 Substitution of another highly conserved lysine residue in nsp8, HCoV-229E pp1a Lys-3711,
549 with Ala resulted in a >90% reduction of RNA-binding activity (Fig. 9B and D), while the
550 TATase activity of this protein was completely abolished using two different substrates (Fig.
551 7A and C). A mutant HCoV-229E full-length RNA containing this particular mutation did not
552 give rise to viable virus following transfection into Huh-7 cells. The HCoV-229E nsp8
553 mutagenesis data are thus in agreement with biochemical data reported for the equivalent
554 substitution in SARS-CoV nsp8 (23) as well as reverse genetics data for this virus. A SARS-
555 CoV mutant containing the equivalent mutation in nsp8 was shown to be crippled and rapidly
556 evolved compensatory mutations to restore near-wildtype growth kinetics in cell culture (14).
557 It should also be mentioned that the complete loss of TATase activity in the HCoV-
558 229E_K3711A protein represents an important control because it excludes potential
559 contaminations with bacterial RNA 3' polyadenylation activities being responsible for the
560 TATase shown in reactions using the recombinant HCoV-229E nsp8 wildtype protein
561 produced and purified under identical conditions.
562
563 In summary, our study is in line with previous reports (12, 23, 24) by showing that
564 coronavirus nsp8 proteins act as nucleotidylyl transferases. However, it does not support
565 previous suggestions on nsp8-associated primase and RdRp activities. Based on our
566 findings, we consider it possible that, in those earlier studies, coronavirus nsp8 polymerase
567 activity data were overinterpreted because two important controls were omitted: (i) there was
568 no proof to show that [$\alpha$-$^{32}$P] GMP (in addition to [$\alpha$-$^{32}$P] AMP) was actually incorporated into
569 product during primed RNA synthesis from a CU template and (ii) no 3'-blocked template
570 RNA was used in *de novo* RdRp assays to exclude the possibility that the presumed full-
571 length transcripts identified in these assays represented 3'-mono- or oligonucleotidylated
572 forms of the template RNA (12, 24). Despite these considerations, we think that the

combined data from this and earlier studies provide sufficient evidence to suggest divalent metal ion-dependent RNA 3' TATase activities for coronavirus nsp8 proteins. This activity is strongly enhanced by the presence of an oligo(U) template strand and can be blocked by substituting a single conserved Lys residue with Ala. While it is clear from this and a previous study that nsp8 is critically involved in coronavirus replication and acts as a cofactor for nsp12-mediated RdRp activity in vitro (14), the diverse functions of nsp8 (both alone and in complex with other replicase subunits) remain to be investigated in more detail, including a possible involvement of the TATase activity in the production of 3'-polyadenylated plus-strand RNAs.

583 **Materials and methods**

584 **Cloning, mutagenesis and protein production**. To produce HCoV-229E nsp8 in
585 *Escherichia coli*, the coding sequence of HCoV-229E pp1a residues 3630-3824 was
586 amplified by reverse transcription-polymerase chain reaction (RT-PCR) from viral RNA
587 isolated from HCoV-229E-infected Huh-7 cells and inserted into pASK3-Ub-CHis$_6$ using
588 restriction- and ligation-free cloning methods (60, 61). The resulting plasmid encoded the full-
589 length HCoV-229E nsp8 fused to an N-terminal ubiquitin tag and a C-terminal His$_6$-tag (25,
590 26). Similarly, the coding sequence of FIPV nsp8 (strain 79/1146; GenBank accession
591 number DQ010921; pp1a residues 3506 to 3700) was inserted into pASK3-Ub-CHis$_6$ plasmid
592 DNA and used to produce an N-terminally ubiquitin-tagged and C-terminally hexahistidine-
593 tagged form of FIPV nsp8. For the production of SARS-CoV nsp8, plasmid pASK3-Ub-nsp8-
594 CHis was used (24). The protein expressed from this plasmid comprised the pp1a residues
595 3920 to 4117 of SARS-CoV (strain Frankfurt-1, Genbank accession number AY291315)
596 fused to an N-terminal ubiquitin tag and a short C-terminal sequence, GSSGHHHHHH,
597 including a hexahistidine tag. For all plasmid constructs, expression was under control of a
598 tet-promoter. Site-specific mutagenesis of plasmid constructs was done using a PCR-based
599 approach (60, 61). Primers used for cloning and mutagenesis are available upon request.
600
601 **Heterologous expression of nsp8 in *E. coli* and protein purification.** For the production
602 of wildtype and mutant coronavirus nsp8 proteins, *E. coli* TB1 cells were used. Bacteria were
603 co-transformed with the appropriate pASK3-Ub expression construct and pCGI plasmid DNA,
604 the latter encoding the ubiquitin-specific carboxyl-terminal hydrolase 1 (Ubp1) (25). LB
605 medium containing ampicillin (100 µg/ml) and chloramphenicol (34 µg/ml) was inoculated
606 with an overnight culture of *E. coli* TB1 cells carrying the appropriate plasmids and the
607 culture was incubated in a shaking incubator at 37°C. At an $OD_{600}$ of 0.4, protein production
608 was induced with anhydrotetracycline (AHT; 200 ng/ml, IBA Lifesciences) and cells were
609 incubated for another 17 hours at 17°C under vigorous shaking. Next, cells were harvested
610 by centrifugation (3000 × *g* for 10 min) and resuspended in ice-cold NP7a buffer (20 mM

611 Tris-Cl, pH 8.0, 250 mM NaCl, 10 mM imidazole and 15 mM β-mercaptoethanol). After
612 addition of lysozyme (1.5 mg/ml), and EDTA-free protease inhibitor cocktail (Roche) and
613 incubation for 30 min on ice, the cells were sonicated (20 x 10 sec pulses) and insoluble
614 material was removed by centrifugation for 30 min at 40,000 × *g* at 4°C. The supernatant
615 was incubated with preequilibrated Ni-NTA agarose beads (Macherey-Nagel) for 2 hrs at 4°C
616 under gentle agitation. The suspension was then loaded onto a disposable filter column and,
617 after washing with 20 ml NP7a buffer and 20 ml buffer NP8a (20 mM Tris-HCl pH 8.0, 250
618 mM NaCl, 20 mM imidazole and 15 mM β-mercaptoethanol), the protein was eluted with
619 NP9a buffer (20 mM Tris-Cl/pH 8.0, 250 mM NaCl, 200 mM imidazole and 15 mM β-
620 mercaptoethanol). Eluate fractions were analyzed by SDS-PAGE and fractions containing
621 nsp8 were pooled and subjected to anion-exchange chromatography using an ÄKTAprime
622 plus instrument (GE Healthcare). To this end, eluate fractions from the Ni-NTA
623 chromatography were diluted tenfold with buffer A (20 mM Tris-Cl/pH 8.0, 5 % v/v glycerol
624 and 10 mM β-mercaptoethanol) and loaded onto a HiTrap Q column (1 ml; GE Healthcare).
625 Nonspecifically bound proteins were removed by washing with 30 ml of A30 buffer (20 mM
626 Tris-Cl/pH 8.0, 30 mM NaCl, 5 % glycerol and 10 mM β-mercaptoethanol) and the
627 recombinant protein was eluted using a continuous NaCl gradient (30 mM to 1 M) in buffer
628 containing 20 mM Tris-Cl/pH 8.0, 5 % glycerol and 10 mM β-mercaptoethanol. Peak fractions
629 containing the desired protein were identified by SDS-PAGE, pooled and dialyzed against
630 storage buffer (50 mM Tris-Cl/pH 8.0, 150 mM NaCl, 45 % glycerol and 15 mM β-
631 mercaptoethanol) and stored at -20°C until further use.
632
633 **Nsp8 activity assay**. For *in vitro* activity assays, the various forms of coronavirus nsp8
634 produced in this study were incubated with single-stranded (ss), double-stranded (ds) and
635 partial-duplex substrate RNAs, respectively. In addition, a range of 3'-biotinylated substrate
636 RNAs were used. Unless stated otherwise in the text, reaction mixtures contained 50 mM
637 Tris-Cl, pH 8.0, 50 mM NaCl, 1 $MgCl_2$, 1% Triton X-100, 1 mM DTT, 1.5 mM β-
638 mercaptoethanol, 4.5% glycerol, 1 μM substrate RNA, 100 μM of the indicated NTP(s), 0.17

639 μM of the indicated [α-$^{32}$P] NTP(s) and 2 μM nsp8. Reactions were incubated for 60 min at
640 30°C and terminated by the addition of sodium acetate (pH 5.2, 300 mM final concentration)
641 and 10 volumes of ice-cold ethanol. Following centrifugation, the air-dried pellets were
642 resuspended in PCR-grade Proteinase K solution (1 mg/ml final concentration, Invitrogen)
643 and incubated at 55°C for 15 min. Reactions were stopped by adding Fu-mix (6 M urea, 80%
644 deionized formamide, 1x TBE, 0.1% [w/v] bromophenol blue, and 0.1% (w/v) xylene cyanol).
645 Following denaturation for 10 min at 65°C, reaction products were separated in 1x TBE-
646 buffered 12 % polyacrylamide gels containing 7 M urea and analyzed by phosphorimaging
647 using a Typhoon 9200 imager (GE Healthcare) and Quantity One software (BioRad).
648
649 **Electrophoretic mobility shift assay (EMSA)**. For RNA-binding assays,
650 denatured/renatured RNAs were used. First, 5'-[$^{32}$P]-labeled RNAs (600 nM) were denatured
651 in STE buffer (10 mM Tris-HCl/pH 8.0, 100 mM NaCl, 1 mM EDTA) at 95°C for 2 min and
652 then put on ice for 3 min. RNA refolding was done at room temperature for 10 min in buffer
653 containing 50 mM Tris-HCl/pH 8.0, 7,5 mM NaCl, 1 mM $MgCl_2$, 1% Triton X-100, 1 mM DTT.
654 Next, the refolded RNA was mixed with nsp8 and incubated on ice for 1 hour. As a control, a
655 reaction was performed in the absence of nsp8. Typical reaction mixtures (10 μl total volume)
656 contained 60 nM RNA, 2 μM nsp8, 55 mM Tris-HCl/pH 8.0, 50 mM NaCl, 1 mM $MgCl_2$, 1%
657 Triton X-100, 1 mM DTT, 1.5 mM β-mercaptoethanol, 4.5% glycerol and 0.1 mM EDTA. After
658 1 hour, the reaction mixtures were loaded onto 0.5× TBE-buffered, non-denaturing 10%
659 polyacrylamide gels containing 5% glycerol and separated at 4°C by electrophoresis at
660 constant voltage (200 V) for 6 hrs. The dried gels were exposed to phosphorimaging screens
661 and products were analyzed using a Typhoon 9200 imager and Quantity One software
662 (BioRad).
663
664 **Substrate RNAs.** Synthetic RNAs used in this study were purchased from Integrated DNA
665 Technologies (IDT). RNA hybrids (10 μM) were prepared by annealing two RNA
666 oligonucleotides with (fully or partially) complementary sequences in STE buffer in a final

volume of 100 µl. The mixture was incubated at 95°C for 5 min and then cooled down slowly to room temperature. Annealed RNA hybrids were stored at -20°C until further use. For sequences of the ribooligonucleotides used in this study, see Figures 4, 5, 6, 8, and 9, respectively. In addition, the following RNAs were used: KR12, 5'-ACUUAAGUACCUUAUC-UAUCUACAGAUA-3'; KR12Bio, 5'-ACUUAAGUACCUUAUCUAUCUACAGAUA-3'-Biotin; KR05, 5'-UAUCUGUAGAUAGAUAAGGUACUUAAGU-3; KR13, 5'-CUUCCGUCUUAUGGC-CAGUCCAAAUAGU-3'.

**Acknowledgments**

The authors would like to thank Dr. Craig E. Cameron, Pennsylvania State University, for providing plasmid pCG1 and Dr. Eric J. Snijder, Leiden University Medical Center, for providing plasmid pASK3-Ub-SARS-CoV-nsp8-Chis$_6$. The authors also thank Dr. Konstantin Ivanov for his contribution to experiments performed at an early stage of this work. The work was supported by grants from the Deutsche Forschungsgemeinschaft (SFB 1021, A01; IRTG 1384) and the BBSRC (BB/G012067/1).

**References**

1. de Groot RJ, Baker SC, Baric R, Enjuanes L, Gorbalenya AE, Holmes KV, Perlman S, Poon L, Rottier PJM, Talbot PJ, Woo PCY, Ziebuhr J. 2012. Family *Coronaviridae*, p 806-828. *In* King AMQ, Adams MJ, Carstens EB, Lefkowitz EJ (ed), Virus Taxonomy. Elsevier, Amsterdam.

2. Zumla A, Hui DS, Perlman S. 2015. Middle East respiratory syndrome. Lancet 386:995-1007.

3. Gorbalenya AE, Enjuanes L, Ziebuhr J, Snijder EJ. 2006. Nidovirales: evolving the largest RNA virus genome. Virus Res 117:17-37.

4. Ziebuhr J. 2008. Coronavirus replicative proteins, p 65-81. *In* Perlman S, Gallagher T, Snijder EJ (ed), Nidoviruses. ASM Press, Washington, DC.

695 5. Masters PS, Perlman S. 2013. *Coronaviridae*, p 825-858. *In* Knipe DM, Howley PM
696 (ed), Fields Virology, 6th ed, vol 1. Lippincott Williams & Wilkins, Philadelphia, PA.
697 6. Snijder EJ, Decroly E, Ziebuhr J. 2016. The Nonstructural Proteins Directing
698 Coronavirus RNA Synthesis and Processing. Adv Virus Res 96:59-126.
699 7. Sevajol M, Subissi L, Decroly E, Canard B, Imbert I. 2014. Insights into RNA
700 synthesis, capping, and proofreading mechanisms of SARS-coronavirus. Virus Res 194:90-
701 99.
702 8. Sola I, Mateos-Gomez PA, Almazan F, Zuniga S, Enjuanes L. 2011. RNA-RNA and
703 RNA-protein interactions in coronavirus replication and transcription. RNA Biol 8:237-248.
704 9. Sola I, Almazan F, Zuniga S, Enjuanes L. 2015. Continuous and Discontinuous RNA
705 Synthesis in Coronaviruses. Annu Rev Virol 2:265-288.
706 10. Lehmann KC, Gulyaeva A, Zevenhoven-Dobbe JC, Janssen GM, Ruben M,
707 Overkleeft HS, van Veelen PA, Samborskiy DV, Kravchenko AA, Leontovich AM, Sidorov IA,
708 Snijder EJ, Posthuma CC, Gorbalenya AE. 2015. Discovery of an essential nucleotidylating
709 activity associated with a newly delineated conserved domain in the RNA polymerase-
710 containing protein of all nidoviruses. Nucleic Acids Res 43:8416-8434.
711 11. Gorbalenya AE, Koonin EV, Donchenko AP, Blinov VM. 1989. Coronavirus genome:
712 prediction of putative functional domains in the non-structural polyprotein by comparative
713 amino acid sequence analysis. Nucleic Acids Res 17:4847-4861.
714 12. Xiao Y, Ma Q, Restle T, Shang W, Svergun DI, Ponnusamy R, Sczakiel G, Hilgenfeld
715 R. 2012. Nonstructural proteins 7 and 8 of feline coronavirus form a 2:1 heterotrimer that
716 exhibits primer-independent RNA polymerase activity. J Virol 86:4444-4454.
717 13. Zhai Y, Sun F, Li X, Pang H, Xu X, Bartlam M, Rao Z. 2005. Insights into SARS-CoV
718 transcription and replication from the structure of the nsp7-nsp8 hexadecamer. Nat Struct
719 Mol Biol 12:980-986.
720 14. Subissi L, Posthuma CC, Collet A, Zevenhoven-Dobbe JC, Gorbalenya AE, Decroly
721 E, Snijder EJ, Canard B, Imbert I. 2014. One severe acute respiratory syndrome coronavirus

722 protein complex integrates processive RNA polymerase and exonuclease activities. Proc
723 Natl Acad Sci U S A 111:E3900-3909.
724 15. Ferron F, Subissi L, Silveira De Morais AT, Le NTT, Sevajol M, Gluais L, Decroly E,
725 Vonrhein C, Bricogne G, Canard B, Imbert I. 2018. Structural and molecular basis of
726 mismatch correction and ribavirin excision from coronavirus RNA. Proc Natl Acad Sci U S A
727 115:E162-E171.
728 16. Minskaia E, Hertzig T, Gorbalenya AE, Campanacci V, Cambillau C, Canard B,
729 Ziebuhr J. 2006. Discovery of an RNA virus 3'->5' exoribonuclease that is critically involved in
730 coronavirus RNA synthesis. Proceedings of the National Academy of Sciences of the United
731 States of America 103:5108-5113.
732 17. Smith EC, Blanc H, Surdel MC, Vignuzzi M, Denison MR. 2013. Coronaviruses
733 lacking exoribonuclease activity are susceptible to lethal mutagenesis: evidence for
734 proofreading and potential therapeutics. PLoS Pathog 9:e1003565.
735 18. Smith EC, Sexton NR, Denison MR. 2014. Thinking Outside the Triangle: Replication
736 Fidelity of the Largest RNA Viruses. Annu Rev Virol 1:111-132.
737 19. Eckerle LD, Becker MM, Halpin RA, Li K, Venter E, Lu X, Scherbakova S, Graham
738 RL, Baric RS, Stockwell TB, Spiro DJ, Denison MR. 2010. Infidelity of SARS-CoV Nsp14-
739 exonuclease mutant virus replication is revealed by complete genome sequencing. PLoS
740 Pathog 6:e1000896.
741 20. Eckerle LD, Lu X, Sperry SM, Choi L, Denison MR. 2007. High fidelity of murine
742 hepatitis virus replication is decreased in nsp14 exoribonuclease mutants. J Virol 81:12135-
743 12144.
744 21. Ulferts R, Ziebuhr J. 2011. Nidovirus ribonucleases: Structures and functions in viral
745 replication. RNA biology 8:295-304.
746 22. Becares M, Pascual-Iglesias A, Nogales A, Sola I, Enjuanes L, Zuniga S. 2016.
747 Mutagenesis of Coronavirus nsp14 Reveals Its Potential Role in Modulation of the Innate
748 Immune Response. Journal of virology 90:5399-5414.

749 23. Imbert I, Guillemot JC, Bourhis JM, Bussetta C, Coutard B, Egloff MP, Ferron F,
750 Gorbalenya AE, Canard B. 2006. A second, non-canonical RNA-dependent RNA polymerase
751 in SARS coronavirus. EMBO J 25:4933-4942.
752 24. te Velthuis AJ, van den Worm SH, Snijder EJ. 2012. The SARS-coronavirus
753 nsp7+nsp8 complex is a unique multimeric RNA polymerase capable of both de novo
754 initiation and primer extension. Nucleic Acids Res 40:1737-1747.
755 25. Gohara DW, Ha CS, Kumar S, Ghosh B, Arnold JJ, Wisniewski TJ, Cameron CE.
756 1999. Production of "authentic" poliovirus RNA-dependent RNA polymerase (3D(pol)) by
757 ubiquitin-protease-mediated cleavage in Escherichia coli. Protein Expr Purif 17:128-138.
758 26. te Velthuis AJ, Arnold JJ, Cameron CE, van den Worm SH, Snijder EJ. 2010. The
759 RNA polymerase activity of SARS-coronavirus nsp12 is primer dependent. Nucleic Acids
760 Res 38:203-214.
761 27. Thiel V, Herold J, Schelle B, Siddell SG. 2001. Infectious RNA transcribed in vitro
762 from a cDNA copy of the human coronavirus genome cloned in vaccinia virus. J Gen Virol
763 82:1273-1281.
764 28. Hafe LA, Keller EB. 1975. The polyadenylate polymerases from yeast. J Biol Chem
765 250:1838-1846.
766 29. Tsiapalis CM, Dorson JW, De Sante DM, Bollum FJ. 1973. Terminal riboadenylate
767 transferase: a polyadenylate polymerase from calf thymus gland. Biochem Biophys Res
768 Commun 50:737-743.
769 30. Balbo PB, Bohm A. 2007. Mechanism of poly(A) polymerase: structure of the
770 enzyme-MgATP-RNA ternary complex and kinetic analysis. Structure 15:1117-1131.
771 31. Moodie SL, Mitchell JB, Thornton JM. 1996. Protein recognition of adenylate: an
772 example of a fuzzy recognition template. J Mol Biol 263:486-500.
773 32. Nobeli I, Laskowski RA, Valdar WS, Thornton JM. 2001. On the molecular
774 discrimination between adenine and guanine by proteins. Nucleic Acids Res 29:4294-4309.
775 33. Arnold JJ, Cameron CE. 1999. Poliovirus RNA-dependent RNA polymerase (3Dpol)
776 is sufficient for template switching in vitro. J Biol Chem 274:2706-2716.

777 34. Neufeld KL, Galarza JM, Richards OC, Summers DF, Ehrenfeld E. 1994.
778 Identification of terminal adenylyl transferase activity of the poliovirus polymerase 3Dpol. J
779 Virol 68:5811-5818.
780 35. Ranjith-Kumar CT, Gajewski J, Gutshall L, Maley D, Sarisky RT, Kao CC. 2001.
781 Terminal nucleotidyl transferase activity of recombinant Flaviviridae RNA-dependent RNA
782 polymerases: implication for viral RNA synthesis. J Virol 75:8615-8623.
783 36. Poranen MM, Koivunen MR, Bamford DH. 2008. Nontemplated terminal
784 nucleotidyltransferase activity of double-stranded RNA bacteriophage phi6 RNA-dependent
785 RNA polymerase. J Virol 82:9254-9264.
786 37. Fullerton SW, Blaschke M, Coutard B, Gebhardt J, Gorbalenya A, Canard B, Tucker
787 PA, Rohayem J. 2007. Structural and functional characterization of sapovirus RNA-
788 dependent RNA polymerase. J Virol 81:1858-1871.
789 38. Rohayem J, Jager K, Robel I, Scheffler U, Temme A, Rudolph W. 2006.
790 Characterization of norovirus 3Dpol RNA-dependent RNA polymerase activity and initiation
791 of RNA synthesis. J Gen Virol 87:2621-2630.
792 39. Tomar S, Hardy RW, Smith JL, Kuhn RJ. 2006. Catalytic core of alphavirus
793 nonstructural protein nsP4 possesses terminal adenylyltransferase activity. J Virol 80:9962-
794 9969.
795 40. Wu W, Wang Z, Xia H, Liu Y, Qiu Y, Liu Y, Hu Y, Zhou X. 2014. Flock house virus
796 RNA polymerase initiates RNA synthesis de novo and possesses a terminal nucleotidyl
797 transferase activity. PLoS One 9:e86876.
798 41. Wang Z, Qiu Y, Liu Y, Qi N, Si J, Xia X, Wu D, Hu Y, Zhou X. 2013. Characterization
799 of a nodavirus replicase revealed a de novo initiation mechanism of RNA synthesis and
800 terminal nucleotidyltransferase activity. J Biol Chem 288:30785-30801.
801 42. Ranjith-Kumar CT, Gutshall L, Kim MJ, Sarisky RT, Kao CC. 2002. Requirements for
802 de novo initiation of RNA synthesis by recombinant flaviviral RNA-dependent RNA
803 polymerases. J Virol 76:12526-12536.

804 43. Huang SG, Klingenberg M. 1996. Two-stage nucleotide binding mechanism and its
805 implications to H+ transport inhibition of the uncoupling protein from brown adipose tissue
806 mitochondria. Biochemistry 35:7846-7854.
807 44. Tabor S, Richardson CC. 1989. Effect of manganese ions on the incorporation of
808 dideoxynucleotides by bacteriophage T7 DNA polymerase and Escherichia coli DNA
809 polymerase I. Proc Natl Acad Sci U S A 86:4076-4080.
810 45. Hofmann MA, Brian DA. 1991. The 5' end of coronavirus minus-strand RNAs contains
811 a short poly(U) tract. J Virol 65:6331-6333.
812 46. Schweizer MP, Chan SI, Ts'o PO. 1965. Interaction and association of bases and
813 nucleosides in aqueous solutions. IV. Proton magnetic resonance studies of the association
814 of pyrimidine nucleosides and their interactions with purine. J Am Chem Soc 87:5241-5247.
815 47. Ts'O PO, Helmkamp GK, Sander C. 1962. Interaction of nucleosides and related
816 compounds with nucleic acids as indicated by the change of helix-coil transition temperature.
817 Proc Natl Acad Sci U S A 48:686-698.
818 48. Ts'o PO, Kondo NS, Schweizer MP, Hollis DP. 1969. Studies of the conformation and
819 interaction in dinucleoside mono- and diphosphates by proton magnetic resonance.
820 Biochemistry 8:997-1029.
821 49. Friedman RA, Honig B. 1995. A free energy analysis of nucleic acid base stacking in
822 aqueous solution. Biophys J 69:1528-1535.
823 50. Norberg J, Nilsson L. 1995. Stacking Free Energy Profiles for All 16 Natural
824 Ribodinucleoside Monophosphates in Aqueous Solution. J Am Chem Soc Journal of the
825 American Chemical Society 117:10832-10840.
826 51. Balbo PB, Meinke G, Bohm A. 2005. Kinetic studies of yeast polyA polymerase
827 indicate an induced fit mechanism for nucleotide specificity. Biochemistry 44:7777-7786.
828 52. Ortin J, Martin-Benito J. 2015. The RNA synthesis machinery of negative-stranded
829 RNA viruses. Virology 479-480:532-544.

830 53. Hwang LN, Englund N, Pattnaik AK. 1998. Polyadenylation of vesicular stomatitis
831 virus mRNA dictates efficient transcription termination at the intercistronic gene junctions. J
832 Virol 72:1805-1813.
833 54. Robertson JS, Schubert M, Lazzarini RA. 1981. Polyadenylation sites for influenza
834 virus mRNA. J Virol 38:157-163.
835 55. Schnell MJ, Buonocore L, Kretzschmar E, Johnson E, Rose JK. 1996. Foreign
836 glycoproteins expressed from recombinant vesicular stomatitis viruses are incorporated
837 efficiently into virus particles. Proc Natl Acad Sci U S A 93:11359-11365.
838 56. Dorsch-Hasler K, Yogo Y, Wimmer E. 1975. Replication of picornaviruses. I.
839 Evidence from in vitro RNA synthesis that poly(A) of the poliovirus genome is genetically
840 coded. J Virol 16:1512-1517.
841 57. Spector DH, Villa-Komaroff L, Baltimore D. 1975. Studies on the function of
842 polyadenylic acid on poliovirus RNA. Cell 6:41-44.
843 58. Larsen GR, Dorner AJ, Harris TJ, Wimmer E. 1980. The structure of poliovirus
844 replicative form. Nucleic Acids Res 8:1217-1229.
845 59. Sheets MD, Wickens M. 1989. Two phases in the addition of a poly(A) tail. Genes
846 Dev 3:1401-1412.
847 60. Yao Z, Jones DH, Grose C. 1992. Site-directed mutagenesis of herpesvirus
848 glycoprotein phosphorylation sites by recombination polymerase chain reaction. PCR
849 Methods Appl 1:205-207.
850 61. Jones DH, Howard BH. 1991. A rapid method for recombination and site-specific
851 mutagenesis by placing homologous ends on DNA using polymerase chain reaction.
852 Biotechniques 10:62-66.
853 62. Sievers F, Wilm A, Dineen D, Gibson TJ, Karplus K, Li W, Lopez R, McWilliam H,
854 Remmert M, Soding J, Thompson JD, Higgins DG. 2011. Fast, scalable generation of high-
855 quality protein multiple sequence alignments using Clustal Omega. Molecular systems
856 biology 7:539.

857 63. Robert X, Gouet P. 2014. Deciphering key features in protein structures with the new
858 ENDscript server. Nucleic acids research 42:W320-324.

859

**Figure legends**

**Fig. 1. Production of HCoV-229E nsp8 in *E. coli*.** A, Multiple sequence alignment of the N-terminal regions of coronavirus nsp8 proteins representing the genera *Alpha*-, *Beta*-, *Gamma*-, and *Deltacoronavirus*, respectively. Sequences were aligned using Clustal Omega (62) and converted using ESPript (63). Black background color indicates invariant residues. Alanine substitutions in HCoV-229E nsp8 generated in this study are indicated by arrows. Numbers indicate positions in the HCoV-229E polyprotein 1a/1ab sequence. SARS-CoV, Severe acute respiratory syndrome coronavirus (AY291315); MERS-CoV, Middle East respiratory syndrome coronavirus (JX869059.2); MHV, Mouse hepatitis virus A59 (NC_001846.1); IBV, Avian infectious bronchitis virus (NC_001451.1); BW-CoV, Beluga whale coronavirus SW1 (NC_010646); WiCoV, Wigeon coronavirus HKU20 (JQ065048); WECoV, White-eye coronavirus HKU16 (JQ065044); FIPV, Feline infectious peritonitis virus (NC_002306); HCoV-NL63, Human coronavirus NL63 (NC_005831); HCoV-229E, Human coronavirus 229E (NC_002645). Secondary structure elements determined by crystal structure analysis of SARS-CoV nsp8 (pdb 2AHM, chain H) (13) are shown above the alignment. **B,** Coomassie brilliant blue-stained 12% SDS-polyacrylamide gel showing the production and purification of HCoV-229E nsp8-CHis$_6$. Lanes 1 and 2, total lysates of *E. coli* TB1 [pCG1] cells transformed with pASK-Ub-nsp8-CHis$_6$ plasmid DNA and grown in the absence (–) or presence (+) of anhydrotetracycline (AHT); lanes 3-5, purified nsp8-CHis$_6$ proteins (wildtype [WT] or variants containing the indicated alanine substitutions of conserved residues). Molecular masses (in kDa) of marker proteins are indicated to the left.

**Fig. 2. RNA 3'-terminal nucleotidyl transferase (TNTase) activity of HCoV-229E nsp8.** Effects of increasing salt concentrations and the presence of metal ions on TNTase activity. **A,** Nsp8 activity assays were performed in reaction buffer supplemented with 2 µM nsp8, 1 µM $U_{18}$ (substrate RNA), 100 µM ATP, 0.17 µM [$\alpha$-$^{32}$P] ATP, 1 mM $MgCl_2$, and varying concentrations of NaCl (36 to 150 mM). **B,** Activity assays were performed in reaction buffer

supplemented with 2 μM nsp8, 50 mM NaCl, 100 μM ATP, 0.17 μM [$\alpha$-$^{32}$P] ATP, 1 μM $U_{18}$ (substrate RNA), and the indicated concentrations of $MgCl_2$ and $MnCl_2$, respectively (0 to 20 mM). **C,** Activity assays were performed in reaction buffer supplemented with 2 μM nsp8, 50 mM NaCl, 100 μM ATP, 0.17 μM [$\alpha$-$^{32}$P] ATP, and 1 μM $U_{18}$ (left panel) or KR07 RNA (right panel), and the indicated divalent metal ions (each at 1 mM). 5'-[$^{32}$P]-labeled RNAs ($U_{18}$, KR07), respectively, were used as 18-nt and 28-nt markers as indicated to the left. Reactions were incubated at 30°C for 60 min. Products were resolved in a TBE-buffered 12% polyacrylamide-7 M urea gel and visualized by phosphorimaging.

**Fig. 3. TATase activity of HCoV-229E nsp8. A,** Reactions in which $A_{18}$ and $U_{18}$, respectively, were used as substrate RNAs. The suffix 'b' indicates 3'-biotinylation of the respective oligoribonucleotide. **B,** Reactions in which oligoribonucleotides KR07, KR07-b, KR12, KR12-b, KR05, and KR13, respectively, were used as substrate RNAs. Nucleotides used in the respective reactions are indicated above the autoradiogram. M, 5'-[$^{32}$P]-labeled RNA markers, with size(s) in nucleotides indicated to the left. –, Reactions performed in the absence of nsp8. Reactions were performed in reaction buffer supplemented with 50 mM NaCl, 1 mM $MgCl_2$, 2 μM nsp8, 100 μM of the indicated NTP (along with 0.17 μM of the respective 5'-[$\alpha$-$^{32}$P]-labeled NTP), and 1 μM of the indicated oligoribonucleotide. Reactions were incubated at 30°C for 60 min. RNA products were resolved in TBE-buffered 12% polyacrylamide-7M urea gels and visualized by phosphorimaging.

**Fig. 4. Effects of varying 3'-terminal nucleotides on HCoV-229E nsp8 TATase activity. A,** RNA substrates used in the TATase assays shown in panels B and C. **B,** TATase assay using 1 μM of KR07, KR07_C28A, KR07_C28U, and KR07_C28G, respectively. **C,** TATase assay using 1 μM of JZR3, JZR_C22A, JZR3_C22U, and JZR_C22G, respectively, as indicated. 5'-[$^{32}$P]-labeled RNAs loaded in lane M were used as markers. Sizes in nucleotides are indicated to the left. –, Reactions performed with RNA KR07 and JZR3, respectively, in

the absence of nsp8. Reactions were incubated at 30°C for 60 min. Products were resolved in TBE-buffered 12% polyacrylamide-7 M urea gels and visualized by phosphorimaging.

**Fig. 5. Primer extension assay.** Nsp8 activity assays were performed using a primer/template substrate (KR01/JTR1) described in an earlier study (24) and a derivative of this substrate in which the bottom strand was 3'-biotinylated (KR01/JTR1-b). **A,** Primer/template RNA hybrids used in this experiment. **'**Bio**'** indicates RNA 3'-biotinylation. **B,** Assays were performed in reaction buffer supplemented with 2 μM nsp8, 50 mM NaCl, 4 mM of $MgCl_2$, 50 μM ATP and/or GTP, 0.17 μM [$\alpha$-$^{32}$P] ATP (*ATP) or [$\alpha$-$^{32}$P] GTP (*GTP) as indicated, and 1 μM of the indicated RNA substrate. Reactions were incubated at 30°C for 60 min. Products were resolved in a TBE-buffered 12% polyacrylamide-7 M urea gel and visualized by phosphorimaging. Sizes (in nucleotides) of 5'-[$^{32}$P]-labeled marker RNAs (lane M) are indicated to the left. –, Activity assay performed with KR01/JTR1 in the absence of nsp8.

**Fig. 6. HCoV-229E nsp8 TATase activities on partially double-stranded substrate RNAs with different 10-nt 5' overhangs. A,** RNA substrates used in this experiment. **'**Bio**'** indicates RNA 3'-biotinylation. **B,** Nsp8 activity assays were performed in standard reaction buffer in the presence of 100 μM ATP and 0.17 μM [$\alpha$-$^{32}$P] ATP using the RNA substrates indicated above. **C,** Nsp8 activity assays were performed in standard reaction buffer using the RNA substrates indicated above the autoradiograms. Reactions were performed in the presence of 100 μM ATP and 0.17 μM [$\alpha$-$^{32}$P] ATP (lanes 1 to 4), 100 μM UTP and 0.17 μM [$\alpha$-$^{32}$P] UTP (lane 5), and 100 μM GTP and 0.17 μM [$\alpha$-$^{32}$P] GTP (lane 6), respectively. Reactions were incubated at 30°C for 60 min. Products were resolved in a TBE-buffered 12% polyacrylamide-7 M urea gel and visualized by phosphorimaging. In lane M, 5'-[$^{32}$P]-labeled oligoribonucleotides were loaded as markers. Sizes (in nucleotides) are indicated.

**Fig. 7. HCoV-229E nsp8 TATase activity on partially double-stranded substrate RNAs with different 20-nt 5' overhangs. A,** RNA substrates used in this experiment. 'Bio' indicates RNA 3'-biotinylation. **B,** Nsp8 activity assays were performed in standard reaction buffer in the presence of 100 μM ATP and 0.17 μM [α-$^{32}$P] ATP using the RNA substrates shown in panel A. Reactions were incubated at 30°C for 60 min. Products were resolved in a TBE-buffered 12% polyacrylamide-7 M urea gel and visualized by phosphorimaging. In lane M, 5'-[$^{32}$P]-labeled ribooligonucleotides were loaded as markers. Sizes (in nucleotides) are indicated to the left.

**Fig. 8. Oligo(U)-templated TATase activities of representative coronavirus nsp8 proteins. A,** RNA substrates used in this experiment. 'Bio' indicates RNA 3'-biotinylation. **B,** Activity assays were performed in standard reaction buffer with the indicated recombinant proteins in the presence of 100 μM ATP and 0.17 μM [α-$^{32}$P] ATP using the substrate RNAs shown in panel A. Reactions were incubated at 30°C for 60 min. Products were resolved in a TBE-buffered 12% polyacrylamide-7 M urea gel and visualized by phosphorimaging (selected lanes from the same autoradiogram are shown). 5'-[$^{32}$P]-labeled oligonucleotides were loaded as markers (lane M). Sizes (in nucleotides) are indicated to the left.

**Fig. 9. TATase and RNA-binding activities of wildtype and mutant forms of HCoV-229E nsp8. A** and **B,** TATase assays performed in standard reaction buffer using the indicated wildtype and mutant HCoV-229E nsp8 proteins and substrate RNAs ($U_{18}$ and KR07, respectively). Products were resolved in TBE-buffered 12% polyacrylamide-7 M urea gels and visualized by phosphorimaging. **C** and **D,** RNA-binding activities of wildtype and mutant HCoV-229E nsp8 proteins with the indicated 5'-[$^{32}$P]-labeled homopolymeric substrate RNAs (**C**) and the heteropolymeric substrate RNA KR07 (**D**), respectively. Products were separated in non-denaturing 10% polyacrylamide gels and visualized by phosphorimaging. The positions of free and protein-bound [$^{32}$P]-labeled RNAs are indicated to the right.

970

971

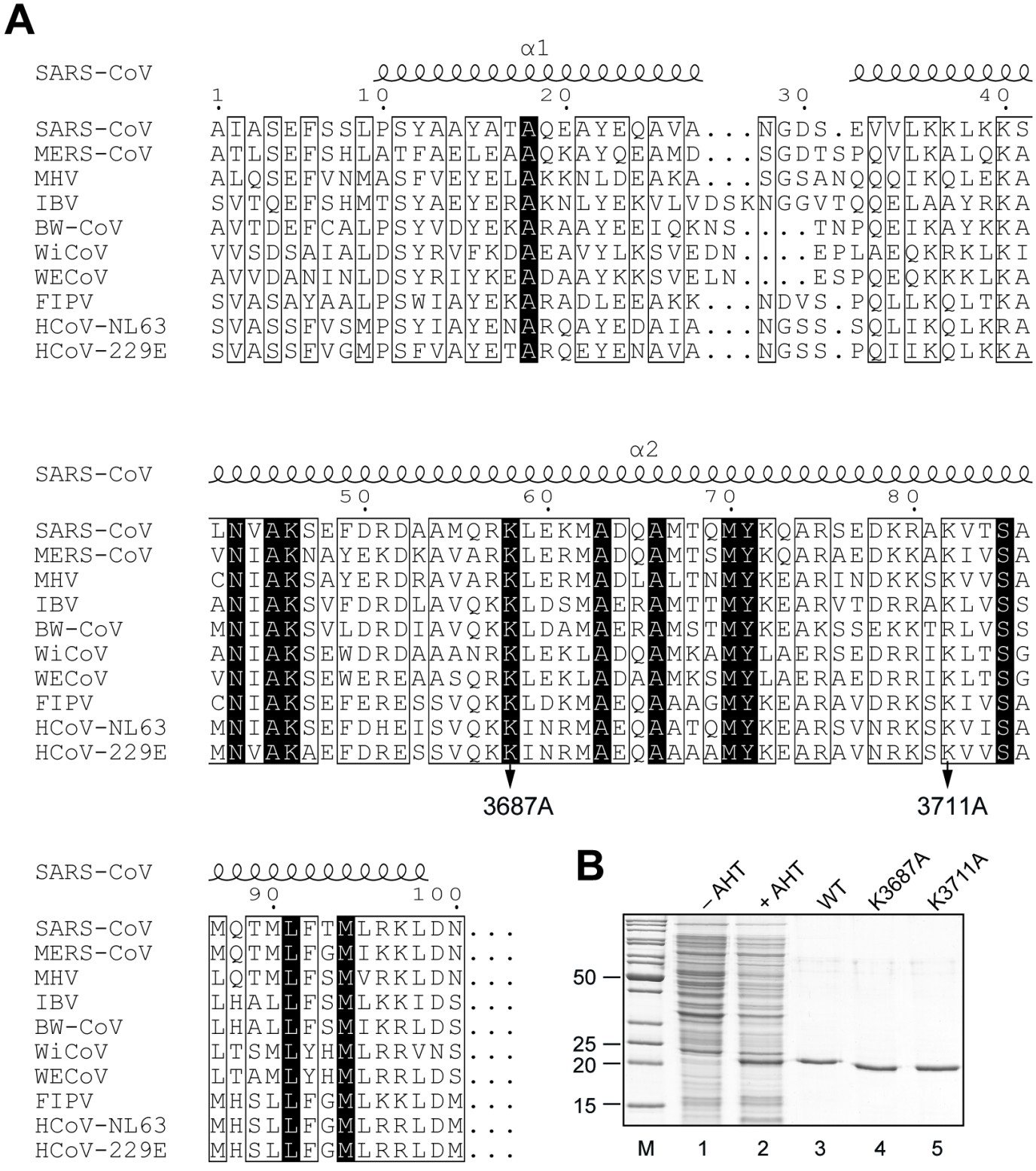

Journal of Virology

JVI

Journal of Virology

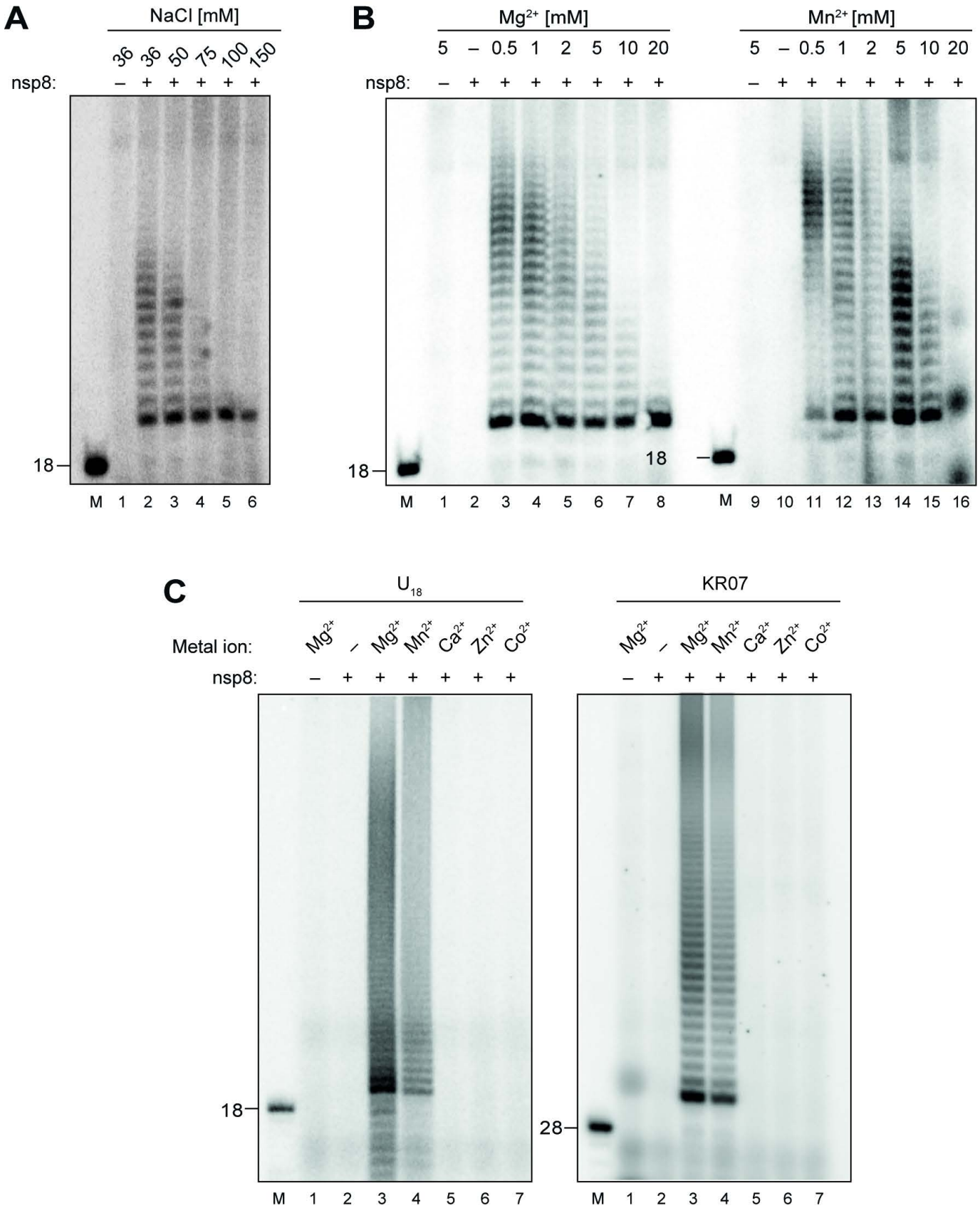

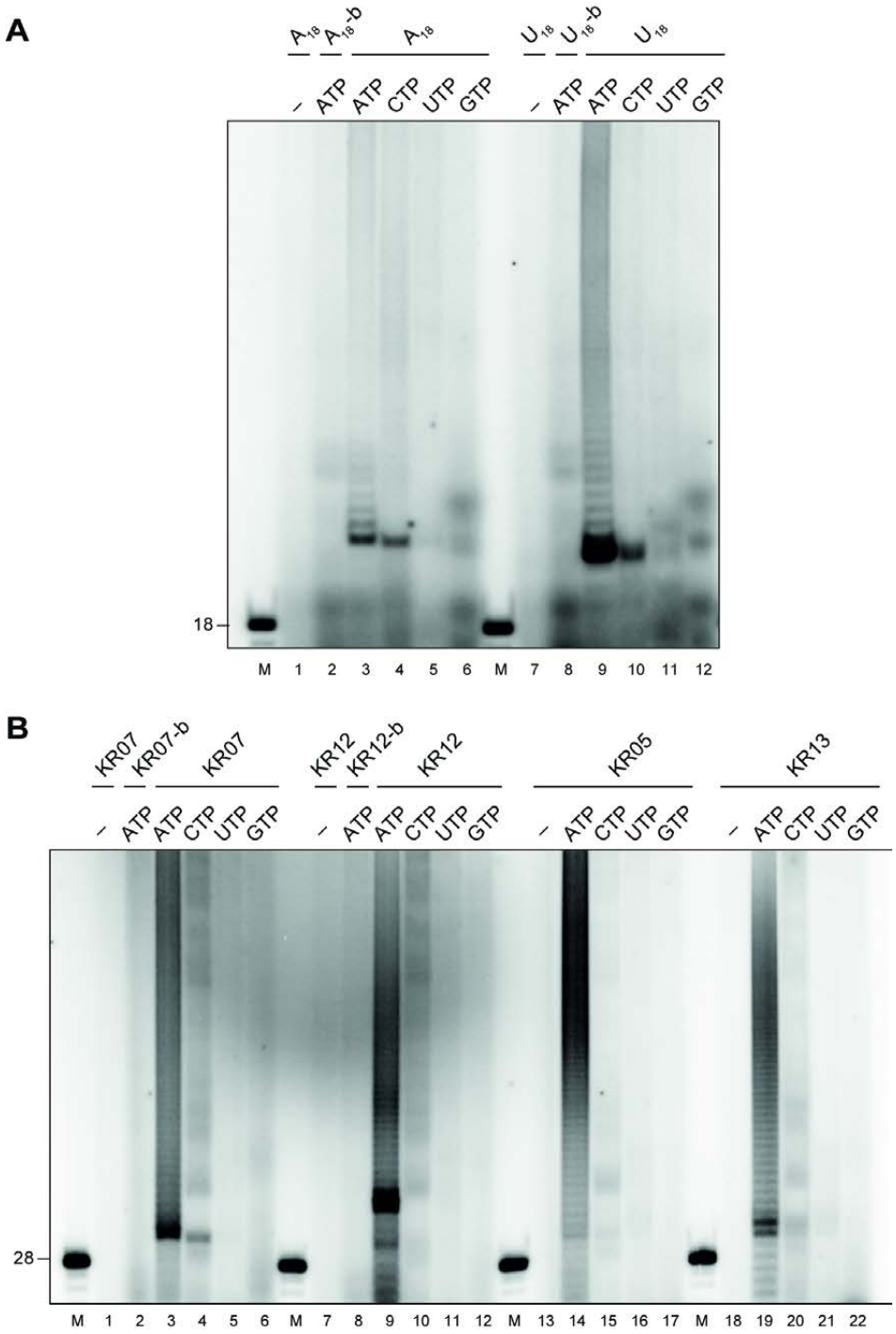

Journal of Virology

JVI

Journal of Virology

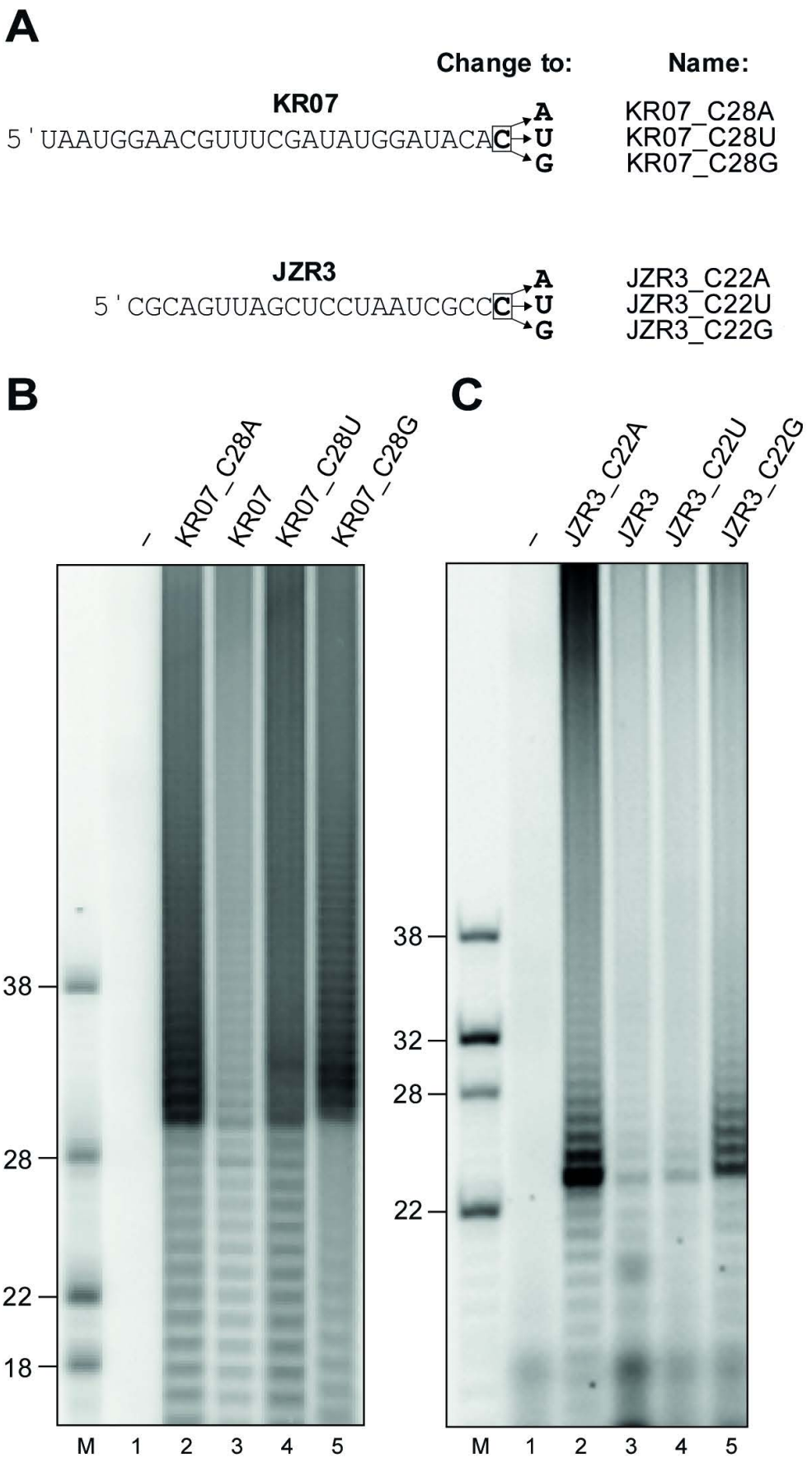

A

**KR01/JTR1**

```
5'-GCUAUGUGAGAUUAAGUUAU-3'
   ||||||||||||||||||||
3'-CGAUACACUCUAAUUCAAUACUCUCUCUCUCUCUCUCUCU-5'
```

**KR01/JTR1-b**

```
5'-GCUAUGUGAGAUUAAGUUAU-3'
   ||||||||||||||||||||
Bio-3'-CGAUACACUCUAAUUCAAUACUCUCUCUCUCUCUCUCUCU-5'
```

B

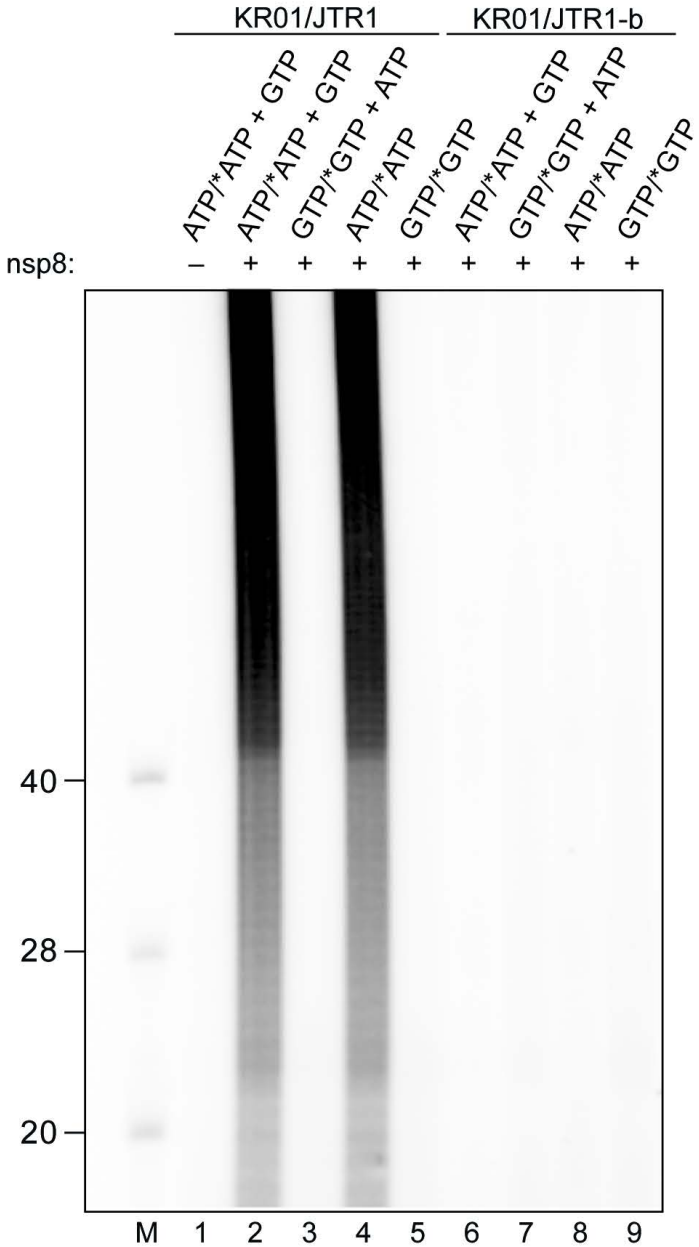

## A

**KR07-b**

```
5'-UAAUGGAACGGUUUCGAUAUGGAUACAC-3'-Bio
```

**KR07**

```
5'-UAAUGGAACGGUUUCGAUAUGGAUACAC-3'
```

**KR07 / KR07comp-b**

```
5'-UAAUGGAACGGUUUCGAUAUGGAUACAC-3 '
   ||||||||||||||||||||||||||||||
Bio-3'-AUUACCUUGCCAAAGCUAUACCUAUGUG-5'
```

**KR07-b / KR07comp-b**

```
5'-UAAUGGAACGGUUUCGAUAUGGAUACAC-3'-Bio
   ||||||||||||||||||||||||||||||
Bio-3'-AUUACCUUGCCAAAGCUAUACCUAUGUG-5'
```

**KR07-b / $U_{10}$KR07comp-b**

```
5'-UAAUGGAACGGUUUCGAUAUGGAUACAC-3'-Bio
   ||||||||||||||||||||||||||||||
Bio-3'-AUUACCUUGCCAAAGCUAUACCUAUGUGUUUUUUUUUU-5'
```

**KR07 / $U_6C_5$KR07comp-b**

```
5'-UAAUGGAACGGUUUCGAUAUGGAUACAC-3'
   ||||||||||||||||||||||||||||||
Bio-3'-AUUACCUUGCCAAAGCUAUACCUAUGUGCCCCCUUUUU-5'
```

**KR07 / $U_{10}$KR07comp-b**

```
5'-UAAUGGAACGGUUUCGAUAUGGAUACAC-3'
   ||||||||||||||||||||||||||||||
Bio-3'-AUUACCUUGCCAAAGCUAUACCUAUGUGUUUUUUUUUU-5'
```

**KR07 / $C_5U_5$-KR07comp-b**

```
5'-UAAUGGAACGGUUUCGAUAUGGAUACAC-3'
   ||||||||||||||||||||||||||||||
Bio-3'-AUUACCUUGCCAAAGCUAUACCUAUGUGUUUUUCCCCC-5'
```

**KR07 / $A_{10}$-KR07comp-b**

```
5'-UAAUGGAACGGUUUCGAUAUGGAUACAC-3'
   ||||||||||||||||||||||||||||||
Bio-3'-AUUACCUUGCCAAAGCUAUACCUAUGUGAAAAAAAAAA-5'
```

**KR07 / $C_{10}$-KR07comp-b**

```
5'-UAAUGGAACGGUUUCGAUAUGGAUACAC-3'
   ||||||||||||||||||||||||||||||
Bio-3'-AUUACCUUGCCAAAGCUAUACCUAUGUGCCCCCCCCCC-5'
```

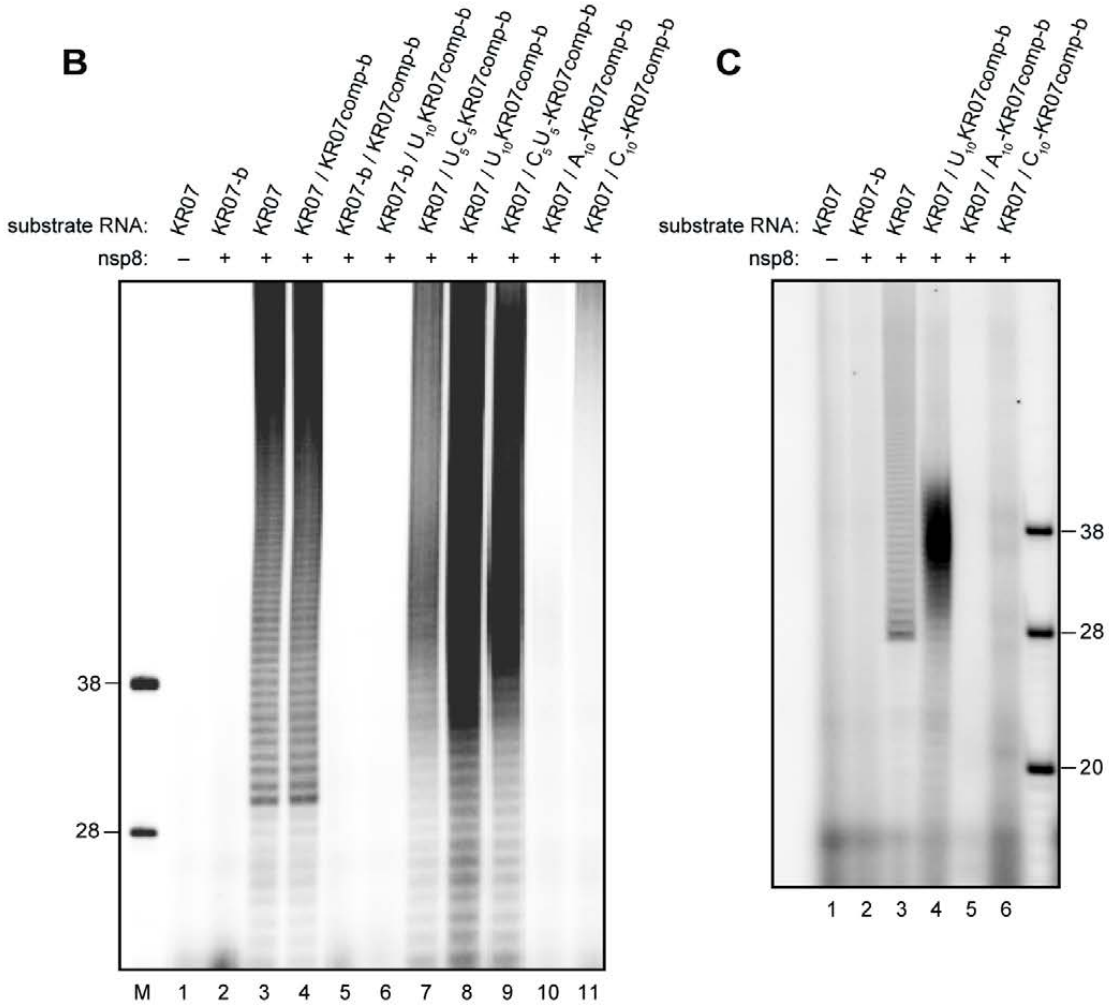

**A**

**1: KR01-b**

5'-GCUAUGUGAGAUUAAGUUAU-3'-Bio

**2: KR01**

5'-GCUAUGUGAGAUUAAGUUAU-3'

**3: KR01 / JTR1-b**

5'-GCUAUGUGAGAUUAAGUUAU-3'
||||||||||||||||||||
**Bio**-3'-CGAUACACUCUAAUUCAAUACUCUCUCUCUCUCUCUCUCU-5'

**4: KR01-b / JTR1-b**

5'-GCUAUGUGAGAUUAAGUUAU-3'-**Bio**
||||||||||||||||||||
**Bio**-3'-CGAUACACUCUAAUUCAAUACUCUCUCUCUCUCUCUCUCU-5'

**5: KR01-b / $U_{20}$JTR1-b**

5'-GCUAUGUGAGAUUAAGUUAU-3'-**Bio**
||||||||||||||||||||
**Bio**-3'-CGAUACACUCUAAUUCAAUAUUUUUUUUUUUUUUUUUUUU-5'

**6: KR01 / $U_{20}$JTR1-b**

5'-GCUAUGUGAGAUUAAGUUAU-3'
||||||||||||||||||||
**Bio**-3'-CGAUACACUCUAAUUCAAUAUUUUUUUUUUUUUUUUUUUU-5'

**B**

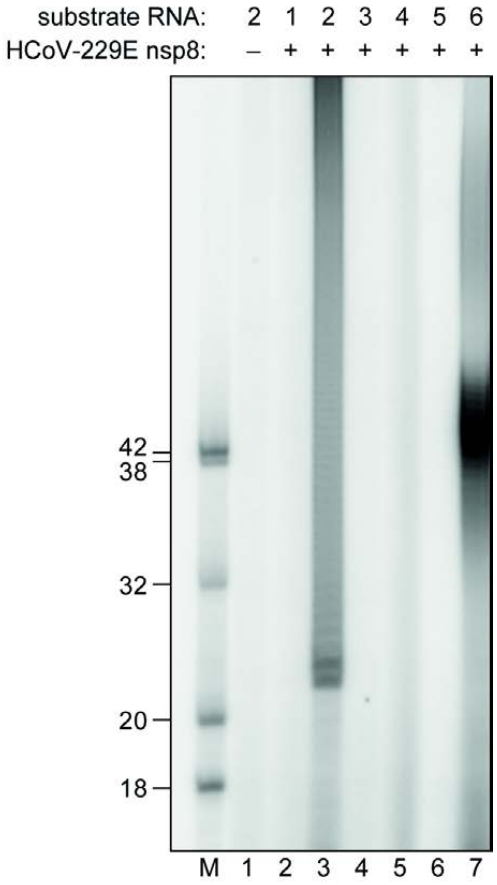

**A**

**5: KR01-b / $U_{20}$JTR1-b**

```
  5'-GCUAUGUGAGAUUAAGUUAU-3'-Bio
     ||||||||||||||||||||
Bio-3'-CGAUACACUCUAAUUCAAUAUUUUUUUUUUUUUUUUUUUU-5'
```

**6: KR01 / $U_{20}$JTR1-b**

```
  5'-GCUAUGUGAGAUUAAGUUAU-3'
     ||||||||||||||||||||
Bio-3'-CGAUACACUCUAAUUCAAUAUUUUUUUUUUUUUUUUUUUU-5'
```

**B**